



TECHNICAL UNIVERSITY OF DENMARK

BACHELOR PROJECT

The Gulf Stream as a Dynamical System

Authors:

Karl Find Hansen - s193624

David Miles-Skov - s204755

Supervisor:

Poul G. Hjorth

December 21, 2023

Preface

The following thesis was prepared at the Department of Applied Mathematics and Computer Science at the Technical University of Denmark as a fulfillment of requirements for acquiring a BSc in General Engineering. The thesis has been done and written in the period from September to November 2023. The project has a total weight of 30 ECTS-points.

David Miles-Skov (s204755)

Signature: _____

Date, Location: _____

Karl Find Hansen (s193624)

Signature: _____

Date, Location: _____

Acknowledgments

We want to express our deepest gratitude to associate professor at DTU Poul G. Hjorth, whom this project was made in collaboration with. We would like to thank Poul for making this project possible, introducing us to the topic and supporting us. We would also like to express gratitude to Henry Stommel for his pioneering work in ocean dynamics, leading to the whole foundation of this thesis.

Gratitude is also extended to Víctor Loras and Unai Lería, whose phaseportrait library has been used extensively throughout this work.

Abstract

The ocean plays a major role in our climate system and in climate change. In this paper we present a conceptual model of the Gulf Stream, an important component of the ocean's global energy transport circulation has, in recent times, been weakening. Using the box-model introduced by Henry Stommel, we explore potential equilibrium states and their real-world implications from a Dynamical Systems perspective. The model exhibits two stable regimes, one having an orientation aligned with today's AMOC, and the other corresponding to a reversal of the AMOC. Another more tailored model building upon the work of Stommel is also devised and explored, exhibiting the more complex interactions between multiple oceanic flows in the North Atlantic along with the consideration of salinity changes due to external environmental conditions.

Contents

1	Introduction	1
2	Theoretical Background	2
2.1	Ocean Currents	2
2.2	Dynamical Systems	3
2.2.1	Saddle-Node Bifurcation	4
2.2.2	Other Bifurcations	5
2.3	The Box-Model	6
2.3.1	One Box-Model	6
2.3.2	Two Box-Model	11
2.3.3	Analysis of System Dynamics	15
3	Three Box-Model	21
3.1	Salinity Anomalies in the Atlantic	21
3.2	Model Description	21
3.2.1	Conceptual Set-Up	22
3.2.2	System of Equations	22
3.2.3	Equilibria and Flow Rates	23
3.3	Bifurcations	26
3.4	Comparisons and Conclusion	27
3.4.1	Comparative Analysis	27
3.4.2	Conclusion	27
	References	29
	Glossary	31
4	Parameters	33
4.1	General parameters	33
4.2	Nondimensional parameters two box model	33
4.3	Nondimensional parameters three box model	34
5	Appendix	34
5.1	Two Box Model	34
5.1.1	Two Box Nondimensionalization	34
5.1.2	Lipschitz Continuity	35
5.1.3	Solutions to system	35
5.1.4	Bifurcation value	36
5.1.5	Using R as bifurcation parameter	37
5.2	Three Box-Model	37
5.2.1	Derivation	37
5.2.2	Symmetrical Salinity Flux	39
5.2.3	Flow Configurations	42

5.2.4	Interpreting Nondimensionalized Flows	42
5.2.5	Equilibria and Stability Analysis	43
5.2.6	High Resolution Phase Portrait at Zero Salinity Flux	46
5.2.7	Bifurcation Figures	47
5.3	GitHub Repository	51

1 Introduction

That the earth's climate is changing is difficult to dispute. The most recent IPCC report concludes that many of the observed changes of the climate are unprecedented. Average temperatures of oceans and atmosphere have increased, total surface coverage of snow and ice has decreased and sea levels have risen [1]. The oceans are pivotal in our climate system, possessing an incredible capacity for absorbing large amounts of CO₂ from the atmosphere. It is estimated that the ocean has absorbed 40% of all human produced CO₂ since the beginning of the industrial era [2]. The focus of this paper lies in the aspects of the oceans role in transporting vast amount of heat and energy around the globe. The thermohaline circulation (THC) is a major global circulation pattern, with oceanic flows that are determined by density contrasts, are ultimately defined by differences in temperature and salinity [3]. One component of the THC is the atlantic meridional overturning circulation abbreviated AMOC, consisting of northward flow of warm ocean water to the North Atlantic, and a deep southward flow of cold denser water, coming from deep water formation at the higher latitudes [4]. Changes of the strength of the AMOC alters the process of heat transport to northern regions, potentially having impacts that could lead to a colder climate in Northern Europe [1, 5, 6].

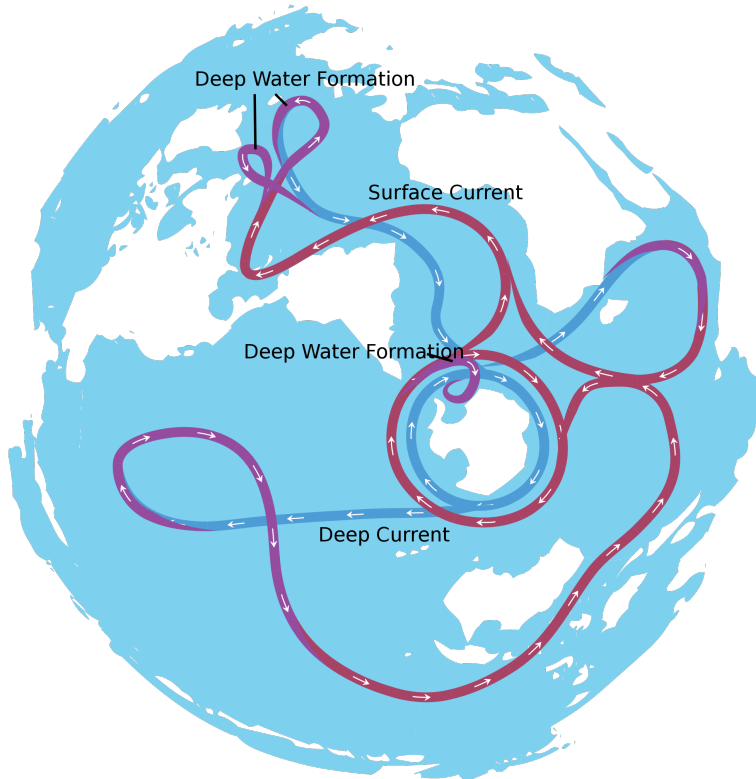


Figure 1: Thermohaline Circulation

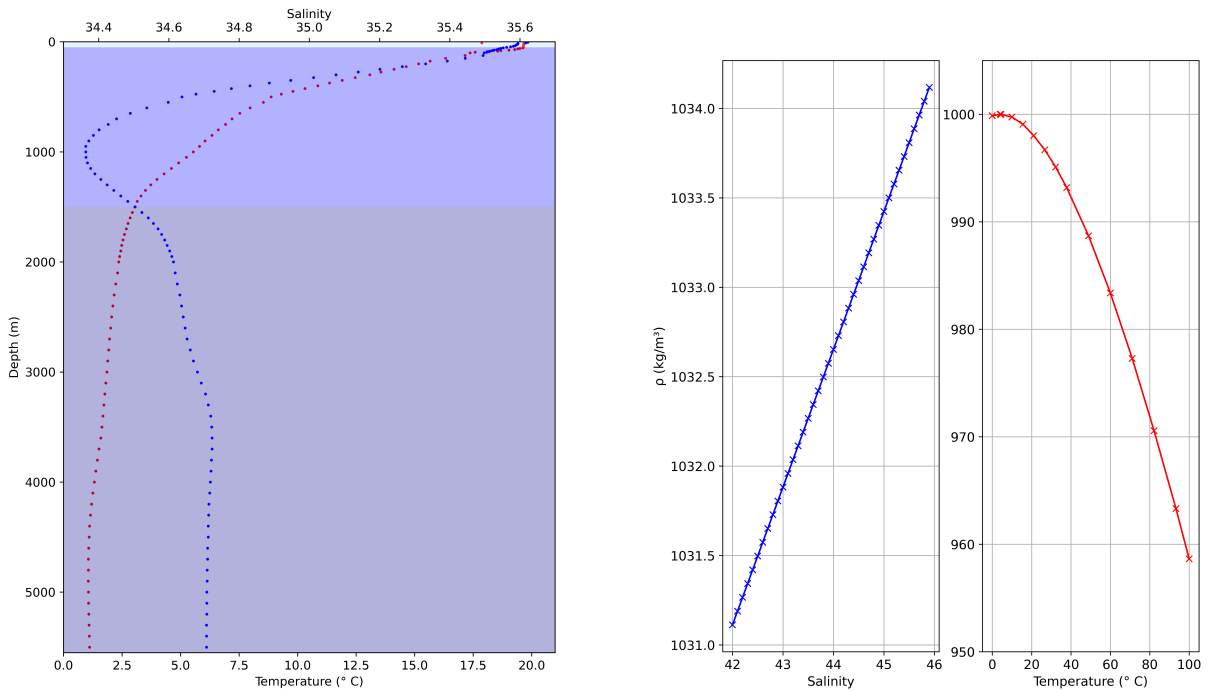
In his pioneering 1961 work, Henry Stommel introduced a conceptual 2-reservoir ocean box-model to investigate the density driven flow between the two boxes representing oceanic

regions of different salinity and temperature [7]. Water flows in an overturning circulation between the two boxes, with the direction and strength of this flow being investigated via the time-dependent relationships between temperature and salinity. Stommel found coexisting stable regimes, one for each direction of the flows leading to the consideration if two such stable regimes can occur in nature. In the following sections the dynamics behind this consideration is investigated, ultimately extending Stommel's two-box model in order to model the Gulf Stream as a component of the North Atlantic part of the AMOC.

2 Theoretical Background

2.1 Ocean Currents

The oceans of the world are important in maintaining a stable climate system. This is due to the unique physical properties of water, allowing it to store and distribute large amounts of heat. Heat is transported across the globe along the oceanic currents. While surface currents are driven mainly by winds, the THC is driven by density contrasts arising from differences in salinity and temperature [3].



(a) Example of oceanic temperature and salinity profile. Data taken from the Pacific ocean, approximately 100km North West of New Zealand's north island [8]. The mixing layer, thermocline and abyssal zone are indicated by increasingly darker shades of blue.

(b) Relationship between water density, temperature [9] and salinity [10]. Clear linear relationship between density and salinity, even at high salinity values. A more complex relationship exists between density and temperature.

Figure 2: Ocean Profile and Water Density

The temperature profile of the oceans can be stratified into three distinct temperature layers. The first layer, known as the *mixing layer* extends to only a few meters in depth. Here, sunlight is a significant factor and the temperature is relatively constant, due to the mixing effect of wind and waves. An intermediate region, the *thermocline*, follows [3]. Temperature in the thermocline decreases somewhat linearly with depth, due to the attenuation of sunlight and up-welling of cold water. The depth of the thermocline varies with latitude, however it generally extends to a depth of around 1km [11]. Lastly, there is the *abyssal zone*, extending to the ocean floor. This layer comprises $\sim 98\%$ [12] of total ocean volume. The temperature here is approximately constant, at a few degrees above freezing. Salinity is the second critical aspect of the density of sea water. Salinity is measured in *practical salinity units*, a dimensionless unit based on conductivity ratios. Values of salinity range from 31 – 39 in the mixed layer but remains close to 35 in the *abyssal zone* [13]. Making sense of the oceanic density contrasts resulting from these relationships is difficult. No equation of state linking density, temperature and salinity exists. As a result, we make use of simple mathematical assumptions to conduct further modelling.

2.2 Dynamical Systems

Dynamical systems is a branch of mathematics that studies the behaviour of systems over time. It provides a foundation for understanding and modeling a wide range of natural phenomena; from its original conception and development during Henri Poincaré's work on the motion of celestial bodies, to the chaotic behaviour of climate systems [14, 15]. It is based on the idea that the behaviour of a system can be described by a set of equations that models its change over time. By characterizing the trajectories that follows the solution of systems through a *phase space*, uncovering the *stable* and *unstable* equilibrium of systems.

Consider the continuous dynamical system described by the ordinary differential equation

$$\dot{x} = f(x, \lambda), \quad f : \mathbb{R}^n \times \mathbb{R} \mapsto \mathbb{R}^n \quad (2.1)$$

Where x is an n-dimensional state vector, f is a *smooth* vector field and λ is some parameter. We assume that the \dot{x} indicates the system's change with respect to time. At steady state, or *equilibrium*, $\dot{x}^* = 0$ where $x^* \in \mathbb{R}^n$ and is known as an *equilibrium/fixed point*. Dynamical systems can have none or multiple equilibrium points, depending on f . Moreover, the position and nature of equilibrium points can change as λ changes. When a suitable change in λ is experienced by the system, the *qualitative structure* of the vector field described by (2.1) changes. This process is known as a *bifurcation*.

A Basic Introduction to Dynamical Systems

Some of the key concepts of dynamical systems can be visualised through the plot of the *nonlinear differential equation*: $\dot{x}(t) = \sin x(t)$.

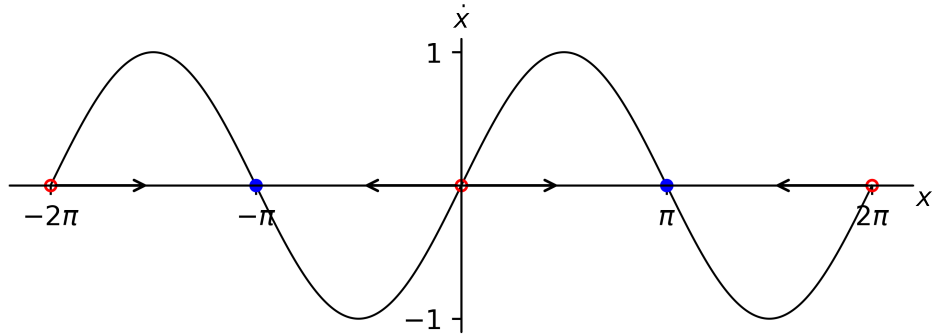


Figure 3: Phase portrait of $\dot{x} = \sin x$. Stable equilibria marked in blue, filled circles, unstable equilibria marked in red, unfilled circles.

If we consider $x(t)$ to represent the displacement of a physical particle, then the figure illustrates the relationship between the particle's displacement and velocity ($\dot{x}(t)$). The *flow of a system* is partially represented by the arrows and dots on the x axis. The dots represent *fixed points*, points at which $\dot{x}^* = 0$, corresponding to stationary motion. These dots are filled when the point is a *stable* fixed point, occurring when $\dot{x}^* < 0$, and are hollow at *unstable* fixed points corresponding to $\dot{x}^* > 0$. The direction of arrows is also determined in a similar way. Arrows will point in the $+x$ direction in regions where $\dot{x}^* > 0$, and in the $-x$ direction where $\dot{x}^* < 0$.

When specific system parameters are varied, new fixed points may arise, existing ones might be destroyed or the stability of existing fixed points changes - qualitative changes known as *bifurcations*. The parameters responsible are known as *bifurcation parameters*. Identifying bifurcation parameters, and altering them provides insight on predicting the behaviour of the system, allowing us to see how the topological structure of the system is changed due to perturbations [16]. Different types of bifurcations arise due to the structure of a dynamical system in relation to its bifurcation parameter. Due to its significance in Stommel's two box-model, we firstly analyse the *saddle-node* bifurcation.

2.2.1 Saddle-Node Bifurcation

The saddle-node bifurcation, also known as a fold bifurcation [16], is a bifurcation in which two fixed points destroy each other. The two fixed points move closer to each other at first, as a parameter is varied, colliding and finally annihilating each other. The saddle-node bifurcation is given by the following *normal form*

$$\dot{x} = f(x, r) = r + x^2 \quad (2.2)$$

where r is the bifurcation parameter. Normal forms of bifurcations provide us with a reference function. All systems containing a saddle

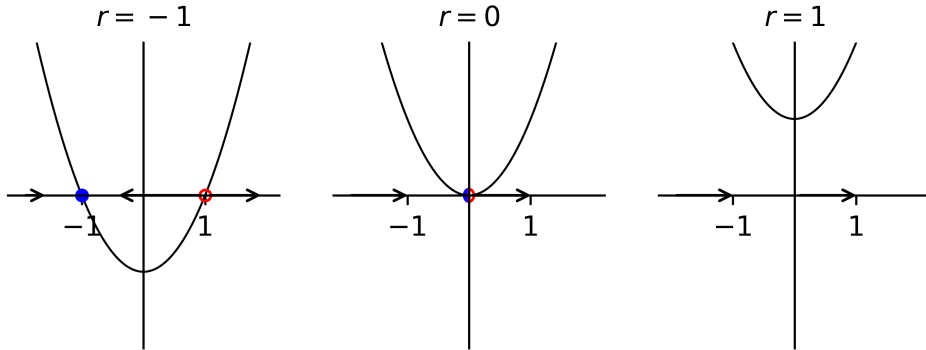


Figure 4: Saddle-node bifurcation for different parameters of r in (2.2). Like in Figure 3 stable equilibria are marked in blue, filled circles, unstable equilibria are marked in red, unfilled circles. When $r < 0$ there is a stable fixed point at $x = -\sqrt{r}$ and an unstable fixed point at $x = +\sqrt{r}$. At the bifurcation point ($r = 0$), there is a saddle-node fixed point. After the collision, at $r > 0$, there are no fixed points.

The system (2.2) has two fixed points at $x^* = \pm\sqrt{r}$ when $r < 0$. From a linear stability analysis of $r < 0$, it can be determined that $x^* = -\sqrt{r}$ is stable as $f'(x^*) = 2x^* = -2\sqrt{r} < 0$ and conversely unstable for $x^* = \sqrt{r}$. For $r = 0$ the two fixed points converge and turn into a single fixed point. This fixed point is referred to as a *half-stable fixed point* or a *saddle-node fixed point*. Half-stable means that the point is stable in one direction and unstable in the other direction. As the parameter r increases beyond 0, the fixed point vanishes, and the system no longer has equilibrium points. The bifurcation can be investigated via a bifurcation diagram, consisting of a locus of fixed points given by $r = -x^2$, with their stability shown.

This visualization allows for tracking the impact of alterations of the parameter r on the overall dynamics of the system. The bifurcation occurs at $r = 0$, where the unstable red line collides with the stable blue line resulting in no equilibrium points for $r > 0$.

2.2.2 Other Bifurcations

Other commonly encountered bifurcations include: *Transcritical* bifurcations, with the normal form $\dot{x} = rx - x^2$, ensuring that a fixed point always exists although with changing stability. *Pitchfork* bifurcations, a normal form of $\dot{x} = rx \pm x^3$ (known as *subcritical* and

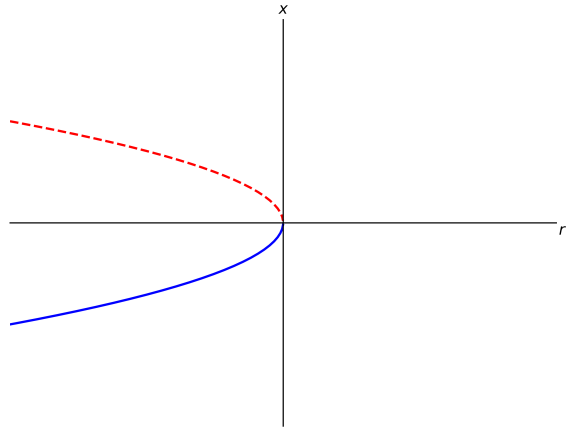


Figure 5: Bifurcation diagram for the saddle-node bifurcation. Stable fixed points are denoted by the blue, continuous line whereas unstable fixed points are denoted by the dashed red line.

supercritical respectively). As the bifurcation parameter is altered, the system goes from one fixed point to three fixed points and vice versa. *Hopf* bifurcations, occurring in two dimensional systems, it is a critical point where the stability of a solution switches and a periodic solution arises. These bifurcations (besides Hopf) are visualised in Figure 6.

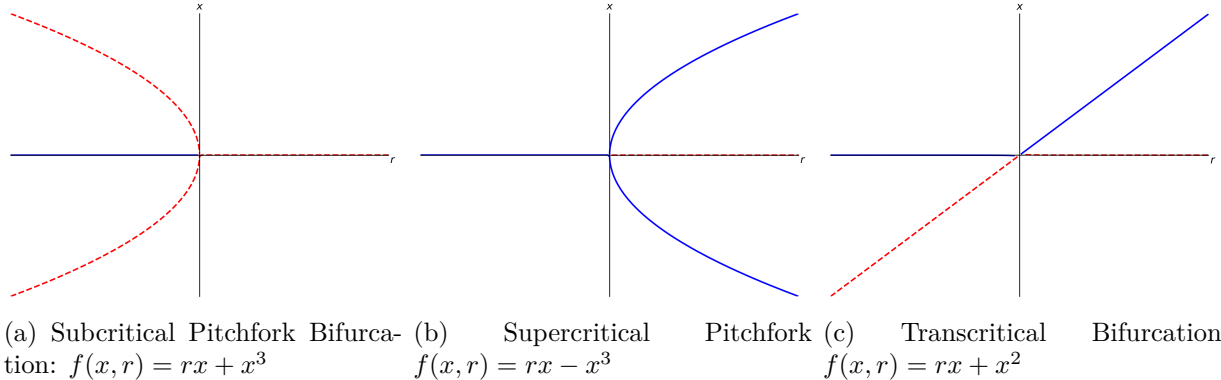


Figure 6: Bifurcation diagrams for subcritical and supercritical pitchfork bifurcations, as well as a transcritical bifurcation. As in Figure 5, unstable fixed points of x are shown by the dashed, red line and stable fixed points are shown by the blue, continuous line.

2.3 The Box-Model

Henry Stommel (1920-1992) [17] was an American oceanographer and meteorologist, known for his contributions to physical oceanography, particularly in circulation patterns and the dynamics of oceans. He was the first scientist to study the changes in the AMOC according to salinity fluxes, devising his *Box-Model* in the process [7]. We will firstly go over the model derivation in detail, as this will serve as the conceptual basis for our further developments and investigation.

2.3.1 One Box-Model

Absent Flow

Let us start with the system shown in Figure 7: A single vessel containing a uniform body of water, with salinity S and temperature T . The vessel is surrounded by two porous walls, and is bounded by another body of water with constant salinity and temperature S^* and T^* respectively. It is further assumed that salinity and heat is transferred through the boundary in a linear manner. We construct the following system of differential equations

$$\dot{T} = c(T^* - T) \quad (2.3a)$$

$$\dot{S} = d(S^* - S) \quad (2.3b)$$

Where c and d are positive constants. We proceed with *nondimensionalizing* the system, allowing us to bypass the need to consider physical values by removing them from the equation via substitution [18]. Introducing the following linear scales

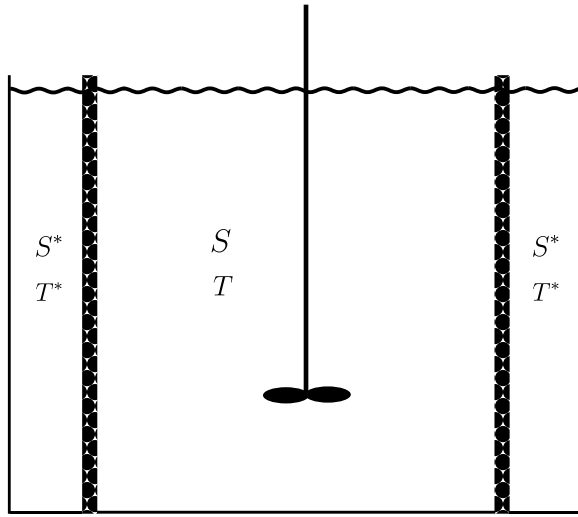


Figure 7: One box-model with no flow. Central reservoir with temperature and salinity of T and S respectively. Separated from two reservoirs with temperature T^* and salinity S^* by porous walls allowing linear transfer of salt and heat. A stirrer is situated in the central reservoir to ensure that the water is well-mixed.

$$\tau = ct, \quad \delta = \frac{d}{c}, \quad y = \frac{T}{T^*}, \quad x = \frac{S}{S^*} \quad (2.4)$$

Resulting in

$$\frac{dy}{d\tau} = \frac{dT}{dt} \cdot \frac{dt}{d\tau} = \frac{1}{c}(c(1 - y)) = 1 - y \quad (2.5a)$$

$$\frac{dx}{d\tau} = \frac{dS}{dt} \cdot \frac{dt}{d\tau} = \frac{1}{c}(d(1 - x)) = \delta(1 - x) \quad (2.5b)$$

If $x(0) = x_0$ and $y(0) = y_0$, the solutions to the above differential equations are

$$y(\tau) = 1 + (y_0 - 1)e^{-\tau} \quad (2.6a)$$

$$x(\tau) = 1 + (x_0 - 1)e^{-\delta\tau} \quad (2.6b)$$

Both solutions have a final equilibrium state of 1 as $\tau \rightarrow \infty$. However, the rate at which this is reached differs due to δ . Salt diffuses more slowly than heat [19] in reality, and the same is assumed for this system. As such, $d < c \Leftrightarrow \frac{d}{c} < 1 \Leftrightarrow \delta < 1$. Following Stommel's work, $\delta = \frac{1}{6}$. We can, therefore, conclude that temperature reaches its asymptotic value more quickly than salinity.

Density Anomaly

To express density in terms of temperature and salinity, an equation of state is required. Owing to the relationships shown in Figure 2b, we make the assumption that density varies

linearly with temperature and salinity around their average values in sea water. Moreover, we know that density is negatively correlated with temperature, due to thermal expansion, but positively correlated with salinity due to mass conservation. Thus, an approximate equation of state is proposed

$$\rho = \rho_0(1 - \alpha T + \beta S) \quad (2.7)$$

Where ρ_0 (g/cm^3) is a reference density achieved at $S = T = 0$. With α ($^{\circ}C^{-1}$) and β being positive average values for the thermal contraction coefficient and saline expansion coefficient, respectively. Expressing this in terms of the nondimensionalized quantities x and y yields

$$\rho = \rho_0(1 + \alpha T^*(-y + Rx)) \quad (2.8)$$

Where $R = \frac{\beta S^*}{\alpha T^*}$ is a dimensionless ratio of the relative effect of salinity and temperature on density. Following Stommel's approach, we are interested primarily in cases where $R > 1$, as this corresponds to the case where density at the final equilibrium state ($x = 1, y = 1$) is higher than that at the initial state ($x = 0, y = 0$). We set $R = 2$, and consider the rate of change of density

$$\dot{\rho} = \rho_0 T(-1 + y + R\delta(1 - x)) \quad (2.9)$$

At the initial state where $x = y = 0$, $\dot{\rho} = \rho_0 \alpha T^*(R\delta - 1) = \rho_0 \alpha T^*(\frac{1}{3} - 1) < 0$. As expected, density is initially decreasing due to the more rapid rate of heat diffusion. The relationship between temperature, salinity and density can be viewed by nondimensionalizing density as expressed in (2.8)

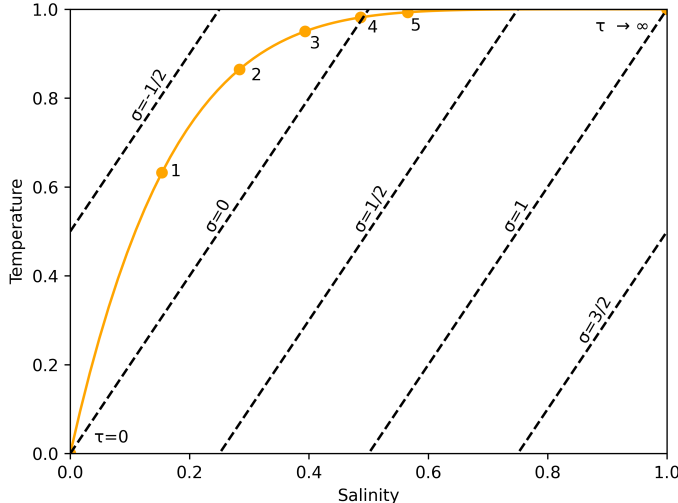


Figure 8: Nondimensionalized temperature vs salinity for $\delta = \frac{1}{6}$ and $R = 2$ in a one-box system. Level sets of constant density anomaly (σ) and points marked on trajectory ϕ_τ (orange curve) at specific values of τ .

$$\sigma = \frac{1}{\alpha T^*} \left(\frac{\rho}{\rho_0} - 1 \right) = -y + Rx \quad (2.10)$$

Stommel refers to σ as a *density anomaly*. Whether water density has increased or decreased is determined by the sign of σ at a certain salinity and temperature. If $\sigma < 0$ density has decreased and vice versa for $\sigma > 0$. Plotting various *level sets* of σ along with the *trajectory* $\phi_\tau = (x(\tau), y(\tau))^T$ allows for clear evaluation of the changes in water density. Examining the graph relative to a density anomaly of 0 ($\sigma = 0$), we can see that density at first decreases, as the trajectory moves away from this level sets. Eventually it begins to increase, reaching and surpassing $\sigma = 0$ at $\tau \approx 4$. At the asymptotic limit $\tau \rightarrow \infty$, the density anomaly is +1.

Introducing Flow - The Steady State Process

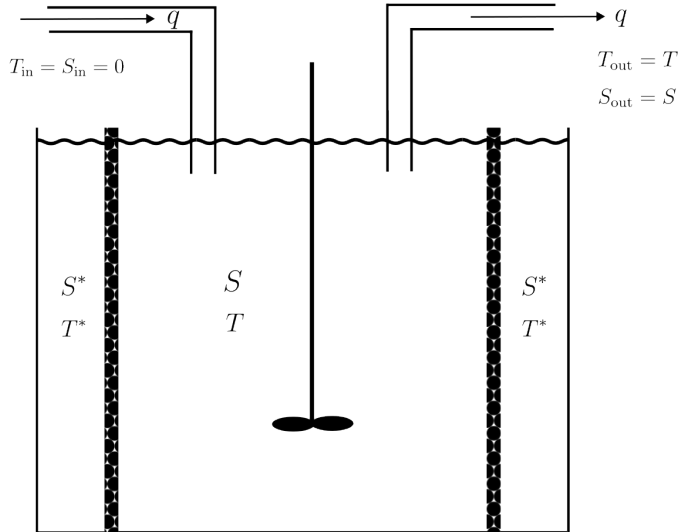


Figure 9: One box-model as in Figure 7 but with flow. Inflow and outflow both of rate q . Inflowing water has temperature $T_{in} = 0$ and salinity $S_{in} = 0$. Outflowing water is water extracted from the central reservoir and therefore $T_{out} = T$ and $S_{out} = S$

We now introduce a flow rate q (s^{-1}) in order to investigate its effect on the density of the system. For simplicity's sake and to avoid an extra system transformation, we assume that there is an inflow $+q$ of water with $T = S = 0$. Mixed water is extracted from the vessel with outflow $-q$. We further define this as a steady state process, where salinity and temperature are kept constant. *I.e.*, $\dot{x} = \dot{y} = 0$. As such, the equations describing the dynamics of the system are

$$\dot{T} = c(T^* - T) - qT = 0 \quad (2.11a)$$

$$\dot{S} = d(S^* - S) - qS = 0 \quad (2.11b)$$

Nondimensionalizing using (2.4)

$$1 - (1 + f')y = 0 \quad (2.12a)$$

$$\delta - (\delta + f')x = 0 \quad (2.12b)$$

Where $f' = \frac{q}{c}$ is a dimensionless flow rate. Finding equilibrium values of x and y

$$y = \frac{1}{1 + f'} \quad (2.13a)$$

$$x = \frac{1}{1 + \frac{f'}{\delta}} \quad (2.13b)$$

Using the common variable of f' , this can now be reformulated into a single equation

$$\frac{1 - y}{y} = \frac{\delta(1 - x)}{x} \quad (2.14)$$

Providing us with a relationship between the equilibrium value of salinity and temperature, which is extracted by the outflowing water

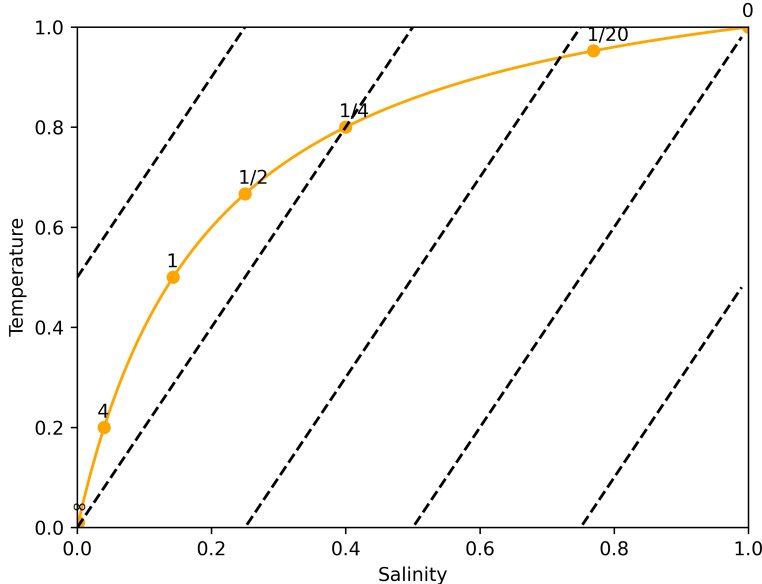


Figure 10: Nondimensionalized temperature vs salinity for $\delta = \frac{1}{6}$ and $R = 2$ in a one-box steady state system. Density anomalies marked as dashed lines as in Figure 8. Various values of f' are marked on the trajectory represented by (2.14). As flow is reduced, the water in the reservoir tends to a nondimensionalized salinity and temperature anomaly of 1.

δ affects the shape of the curve, due to it being a ratio of the diffusivities of salinity and temperature. The variation of flow rate relates to a varying amount of time that inflowing water spends in the vessel, accumulating salinity and temperature. As such, higher flow

rates are associated with lower absolute density anomalies and vice versa. The relationship between salinity, temperature and density has been investigated for a stationary body of water, and a body of water with an inflow and outflow. If we are to use the box-model to describe the AMOC and, more specifically, the Gulf Stream, a system of coupled bodies of water must be considered.

2.3.2 Two Box-Model

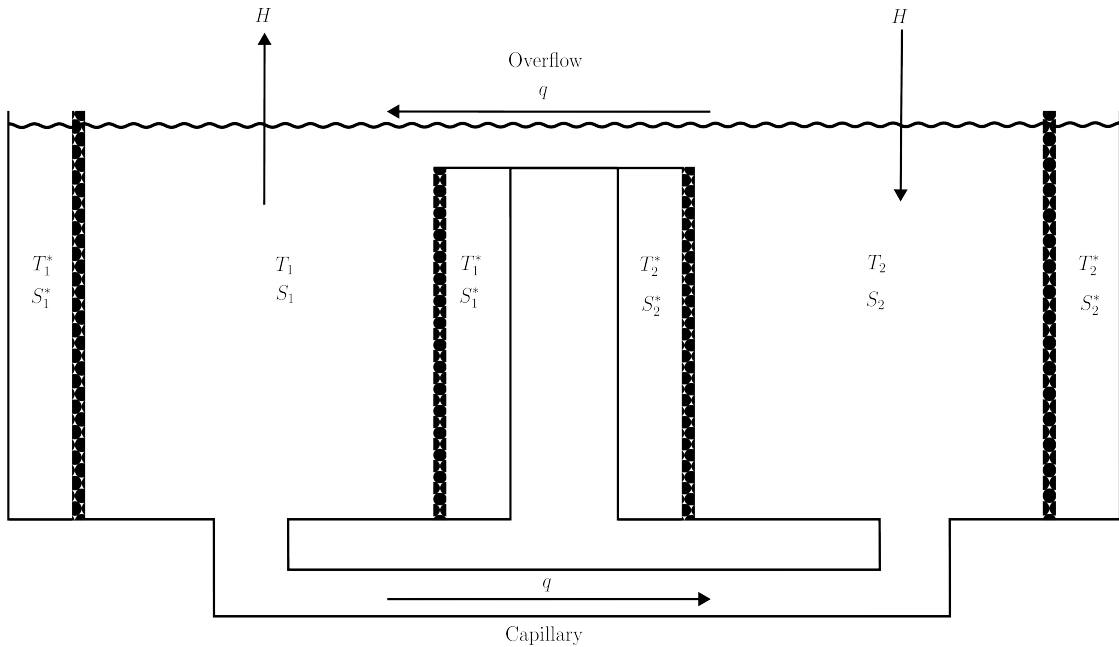


Figure 11: Schematic diagram of the two box-model. Rate of flow, q , through capillary is determined by the density difference between the two boxes. The strength of the overflow is equal to that of the capillary flow so that the surface level in each box remains the same. The density difference between the two boxes depends on the flow rate as well as the temperature and salinity of the transfer through the porous walls.

We now consider Stommel's *two box-model*. Here, two boxes are connected via a capillary tube at the bottom and have a corresponding overflow at the surface to maintain the same volume in each box. There is an exchange of heat and salinity with basins surrounding the boxes having constant temperature T_i^* and salinity S_i^* , $i = 1, 2$, as shown in Figure 11. Let $T_i(t)$ and $S_i(t)$ denote the temperature and salinity in box i at time t . As in the previous models, temperature and salinity in the two boxes is uniform. However, they are not necessarily equal. Density differences in fluids drive convection, leading to fluid motion as lighter, warmer fluid rises and denser, cooler fluid sinks. For example if $S_1 = S_2$, temperature is

the deciding factor on the direction and strength of the overturning circulation. The colder box will contain denser water than the warmer box, and the bottom flow would be from the colder box to the warmer box. This is analogous to a bottom flow from colder, higher latitudes to warmer, lower latitudes. If $T_1 = T_2$, salinity becomes the deciding factor - a situation heavily investigated in later sections 3.1.

Let us consider the effects of evaporation, surface run-off and precipitation. Evaporating water is of zero salinity, giving the remaining water a relatively higher salinity [3, 4]. If the effects of evaporation exceeds that of surface run-off and precipitation, the water experiences a net loss of fresh water and a subsequent increase in salinity. The converse happens to the box where surface run-off and precipitation exceeds evaporation. This is represented by the concept of *virtual salt flux*, H , and leaves a virtual salt flux into the equatorial box and a virtual salt flux out of the polar box. This is analogous to the real-world, where waters at lower latitudes experience a salinity influx due to greater levels of evaporation. Waters at higher latitudes are much colder than waters at lower latitudes, meaning we cannot determine the direction of flow by only considering the effect of either temperature or salinity on density alone [3]. We must consider their combined effect on water density. The flow in the capillary tube is driven by the pressure differences at the bottom of the two boxes, this is proportional to the density differences. Let ρ_1 and ρ_2 be the density in Box 1 and Box 2. The flow in the capillary pipe can be given by the simple linear law

$$q = k \cdot \frac{\rho_1 - \rho_2}{\rho_0} \quad (2.15)$$

The hydraulic constant k (s^{-1}) is a parameterization of various conditions influencing the flow, such as bottom friction and wind driven turbulence in the mixing layer [3]. The sign convention used in (2.15) indicates that $q > 0$, representing the surface flow towards the higher latitudes, implying a bottom flow towards the lower latitudes. And as in (2.7), ρ_0 is a reference density, corresponding to the density when both temperature and salinity are at their average values, defined as

$$T_{avg} = \frac{1}{2}(T_1 + T_2) \quad (2.16a)$$

$$S_{avg} = \frac{1}{2}(S_1 + S_2) \quad (2.16b)$$

In order to find an equation of state for density, we extend the previous equation of state outlined in the one box-model (2.7) for the two box-model

$$\rho_1 = \rho_0(1 - \alpha(T_1 - T_{avg}) + \beta(S_1 - S_{avg})) \quad (2.17a)$$

$$\rho_2 = \rho_0(1 - \alpha(T_2 - T_{avg}) + \beta(S_2 - S_{avg})) \quad (2.17b)$$

Substituting (2.17) into (2.15) results in the following relationship between flow, temperature and salinity

$$q = k \cdot (\alpha(T_2 - T_1) - \beta(S_2 - S_1)) = k(\alpha\Delta T - \beta\Delta S) \quad (2.18)$$

Where $\Delta T = T_2 - T_1$ and $\Delta S = S_2 - S_1$. Due to q being a vector quantity, a change in sign corresponds to a change in direction of the flow. The governing equations for temperature and salinity change are very similar to (2.11), but with minor adjustments: The addition of virtual salt flux H , and compensating for the vector nature of q by using $|q|$

$$\dot{T}_1 = c(T_1^* - T_1) + |q|(T_2 - T_1) \quad (2.19a)$$

$$\dot{S}_1 = H + d(S_1^* - S_1) + |q|(S_2 - S_1) \quad (2.19b)$$

$$\dot{T}_2 = c(T_2^* - T_2) + |q|(T_1 - T_2) \quad (2.19c)$$

$$\dot{S}_2 = -H + d(S_2^* - S_2) + |q|(S_1 - S_2) \quad (2.19d)$$

As the porosity of all the walls is identical, we can consider the rate of change of both the average reservoir temperature and salinity (T_{avg} , S_{avg}), along with the average boundary temperature and salinity (T_{avg}^* , S_{avg}^*)

$$\dot{T}_{\text{avg}} = c(T_{\text{avg}}^* - T_{\text{avg}}) \quad (2.20a)$$

$$\dot{S}_{\text{avg}} = d(S_{\text{avg}}^* - S_{\text{avg}}) \quad (2.20b)$$

Here $T_{\text{avg}}^* = \frac{1}{2}(T_1^* + T_2^*)$ and $S_{\text{avg}}^* = \frac{1}{2}(S_1^* + S_2^*)$. These equations show that both the average salinity and temperature tends to that of the surrounding basins as $t \rightarrow \infty$. As such, we use these average boundary values as reference values and introduce temperature and salinity *anomalies*

$$\bar{T}_1 = T_1 - T_{\text{avg}}^*, \quad \bar{T}_2 = T_2 - T_{\text{avg}}^* \quad (2.21a)$$

$$\bar{S}_1 = S_1 - S_{\text{avg}}^*, \quad \bar{S}_2 = S_2 - S_{\text{avg}}^* \quad (2.21b)$$

Incorporating anomaly quantities into equation (2.19)

$$\dot{\bar{T}}_1 = \dot{T}_1 = c(T_1^* - \bar{T}_1 - T_{\text{avg}}^*) + |q|(\bar{T}_2 - \bar{T}_1) \quad (2.22a)$$

$$\dot{\bar{S}}_1 = \dot{S}_1 = -H + d(S_1^* - \bar{S}_1 - S_{\text{avg}}^*) + |q|(\bar{S}_2 - \bar{S}_1) \quad (2.22b)$$

$$\dot{\bar{T}}_2 = \dot{T}_2 = c(T_2^* - \bar{T}_2 - T_{\text{avg}}^*) + |q|(\bar{T}_1 - \bar{T}_2) \quad (2.22c)$$

$$\dot{\bar{S}}_2 = \dot{S}_2 = H + d(S_2^* - \bar{S}_2 - S_{\text{avg}}^*) + |q|(\bar{S}_1 - \bar{S}_2) \quad (2.22d)$$

By letting $T^* = T_1^* - T_{\text{avg}}^*$ and $S^* = S_1^* - S_{\text{avg}}^*$, we note that $T_2^* - T_{\text{avg}}^* = -T^*$ and $S_2^* - S_{\text{avg}}^* = -S^*$. Substituting this into system (2.22) we get

$$\dot{\bar{T}}_1 = c(T^* - \bar{T}_1) + |q|(\bar{T}_2 - \bar{T}_1) \quad (2.23a)$$

$$\dot{\bar{S}}_1 = -H + d(S^* - \bar{S}_1) + |q|(\bar{S}_2 - \bar{S}_1) \quad (2.23b)$$

$$\dot{\bar{T}}_2 = c(-T^* - \bar{T}_2) + |q|(\bar{T}_1 - \bar{T}_2) \quad (2.23c)$$

$$\dot{\bar{S}}_2 = H + d(-S^* - \bar{S}_2) + |q|(\bar{S}_1 - \bar{S}_2) \quad (2.23d)$$

The advantage of this new system (in terms of anomalies and averages) is that we are only dealing with single constants S^* and T^* . In his original workings Stommel did not

account for evaporation nor precipitation, leading to a virtual salt flux of zero, $H = 0$ [7], the system (2.23) can be reduced accordingly.

Note that the addition of the equations (2.23a) and (2.23c) yields $\dot{\bar{T}}_1 + \dot{\bar{T}}_2 = -c(\bar{T}_1 + \bar{T}_2)$. We see that for any initial conditions $(\bar{T}_1 + \bar{T}_2)(t) \rightarrow 0$ as $t \rightarrow 0$. We will simplify this by assuming $\bar{T}_1 = -\bar{T}_2 = T$. Similarly, addition of (2.23b) and (2.23d) yields $\dot{\bar{S}}_1 + \dot{\bar{S}}_2 = -d(\bar{S}_1 + \bar{S}_2)$. Hence, for any initial conditions $(\bar{S}_1 + \bar{S}_2)(t) \rightarrow 0$ as $t \rightarrow 0$, now assuming $\bar{S}_1 = -\bar{S}_2 = S$. Substituting these changes into (2.23a) and (2.23b) results in the two dimensional system of equations

$$\dot{T} = c(T^* - T) - 2|q|T \quad (2.24a)$$

$$\dot{S} = d(S^* - S) - 2|q|S \quad (2.24b)$$

The solution to the system (2.24) yields the temperature and salinity for the water in box one as a function of time. These characteristics will be mirrored in box two, due to the assumed symmetrical nature of the system. As has been done in the previous one box-model, we proceed with nondimensionalizing the parameters using the linear scales outlined in (2.4), intermediate steps can be seen in (A.1) and (A.2)

$$\dot{x} = \delta(1 - x) - |f|x \quad (2.25a)$$

$$\dot{y} = 1 - y - |f|y \quad (2.25b)$$

Where \cdot denotes $\frac{d}{d\tau}$, $\delta = \frac{d}{c}$ and $f = -\frac{2q}{c}$. The quantity f is a nondimensionalized flow rate. Following assumptions made in (2.17) and the symmetrical relationship between the two boxes ($-\bar{T}_2 = \bar{T}_1 = T$ and $-\bar{S}_2 = \bar{S}_1 = S$), the relationship between flow rate q and density ρ can be investigated in terms of our nondimensionalized variables

$$\begin{aligned} q &= k\rho_0(1 - \alpha\bar{T}_1 + \beta\bar{S}_1) - k\rho_0(1 - \alpha\bar{T}_2 + \beta\bar{S}_2) \\ &= k\rho_0(-\alpha(\bar{T}_1 - \bar{T}_2) + \beta(\bar{S}_1 - \bar{S}_2)) \\ &= k\rho_0(-2\alpha T + 2\beta S) \\ &= 2k\rho_0(-\alpha T + \beta S) \\ &= 2k\rho_0\alpha T^*(-y + Rx) \end{aligned} \quad (2.26)$$

The flow rate, q , is a function of salinity, x , and temperature, y . If temperature dominates the density difference, we have $y > Rx$. As a result, q will be negative; this corresponds to a reverse of the typical configuration of surface flow from warmer waters to colder waters (as exhibited in the AMOC). If salinity dominates the density difference, having $Rx > y$, then q is positive and the capillary flow is in the same direction as exhibited in the AMOC, and water flows from the saltier to the less salty box.

The above relation allows f to be written as

$$\lambda f(x, y) = Rx - y \quad \text{where} \quad \lambda = \frac{c}{2\rho_0\alpha T^*} \quad (2.27)$$

Re-writing (2.25) using the new expression of f

$$\dot{x} = \delta(1 - x) - \frac{1}{\lambda}|y - Rx|x \quad (2.28a)$$

$$\dot{y} = 1 - y - \frac{1}{\lambda}|y - Rx|y \quad (2.28b)$$

We now have three nondimensionalized equations linking salinity, temperature and flow rate. While the system has discontinuities in the second-derivatives of x and y , and are consequently not continuously differentiable, the vector field defined by (2.28) is Lipschitz continuous (A.4, A.5), guaranteeing the existence and uniqueness of the solution to an initial value problem as a result of the Cauchy-Lipschitz theorem [20].

2.3.3 Analysis of System Dynamics

Equilibria

Finding and examining equilibrium states in a dynamical system is essential to understanding how the system behaves under various conditions and can allow us to determine the qualitative features of the system as time progresses. We find the equilibrium points $(x^*, y^*)^T$ of (2.25)

$$\dot{x} = \delta(1 - x^*) - |f|x^* = 0 \quad (2.29a)$$

$$\dot{y} = 1 - y^* - |f|y^* = 0 \quad (2.29b)$$

Subsequently,

$$x^* = \frac{\delta}{\delta + |f|}, \quad y^* = \frac{1}{1 + |f|} \quad (2.30)$$

Using equation (2.27) we obtain the following

$$\lambda f = -y^* + Rx^* = -\frac{1}{1 + |f|} + \frac{R\delta}{\delta + |f|} \equiv \phi(f, R, \delta) \quad (2.31)$$

Solutions from (2.27) for the flow rate f can then be substituted into (2.29a) to determine the equilibrium points. This is investigated in Figure 12, where the intersections represent the equilibrium states. For most values of δ , λ and R there is only one point of intersection, located in the right half-plane when $f > 0$. If λ is sufficiently small there are three points of intersection for certain combinations of δ and R . A condition for identifying three points of intersection is when the graph of $f \rightarrow \phi(f, \delta, R)$ falls below the horizontal axis, $\phi(f) = 0$ for some $f > 0$. Let us explore the limitations of $\phi(f) = 0$

$$\begin{aligned} |f| &= \frac{\delta(R - 1)}{1 - \delta R} \\ \Rightarrow (1 - R)\delta &= (R\delta - 1)|f| \end{aligned}$$

The necessary condition for three points of intersections is

$$R\delta < 1 \quad \text{if} \quad R > 1$$

$$R\delta > 1 \quad \text{if} \quad 0 < R < 1$$

We continue under Stommel's conditions, with $R > 1$ and $\delta < \delta R < 1$. To have three points of intersection λ must also be small enough.

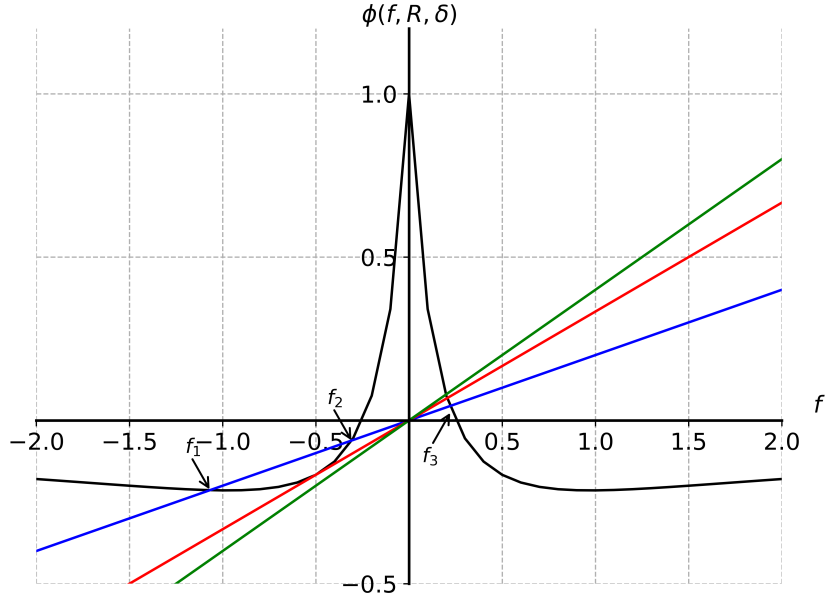


Figure 12: Finding equilibrium flow rates for Stommel's Two Box Model. *Black:* Plot of $\phi(f, R, \delta)$ with $R = 2$, $\delta = \frac{1}{6}$. Lines are plots of $f \rightarrow \lambda f$ with $\lambda = \frac{1}{5}$ (blue), $\lambda = \frac{1}{3}$ (red) and $\lambda = \frac{2}{5}$ (green). Equilibrium flow rates $f_1 = -1.068$, $f_2 = -0.307$ and $f_3 = 0.219$ are identified for $\lambda = \frac{1}{5}$. For $f_1 < 0$ and $f_2 < 0$, the temperature dominates the density difference, resulting in a capillary flow from the cold to the warm box. Conversely, for $f_3 > 0$ the salinity dominates the capillary flow, causing the flow to be from the warm to the cold box.

The black curve in Figure 12 represents the plot of $\phi(f, 2, \frac{1}{6})$, while the blue line represents the graph of λf for $\lambda = \frac{1}{5}$. Here the intersections of the two graphs are the solutions of the substitution of (2.27) into (2.29a). It has three solutions, denoted $f_1 = -1.068$, $f_2 = -0.307$ and $f_3 = 0.219$. While the corresponding equilibrium solutions are denoted (x_i^*, y_i^*) , $i = 1, 2, 3$. Given that $f_1 < 0$ and $f_2 < 0$, the temperature dominates the density difference, and at equilibrium the flow through the capillary is from the cold to the warm box. At $f_3 > 0$ the salinity dominates the density differences, the capillary flow is now from the warm to the cold box.

Stability Analysis

In order to examine the stability of the equilibrium states we proceed by utilising the *Hartman-Grobman theorem* [21], as the equilibrium point (x^*, y^*) is *hyperbolic*. In essence, the theorem states that the linearized system about a critical point is a sufficient approximation of the qualitative structure of the nonlinear system (2.28). The matrix A is calculated

as the *Jacobian* matrix at the critical point, by letting $f^* = f(x^*, y^*) = \frac{Rx^*-y^*}{\lambda}$

$$\begin{pmatrix} \dot{\xi} \\ \dot{\eta} \end{pmatrix} = \begin{pmatrix} -\delta - |f| \pm \frac{Rx^*}{\lambda} & \pm \frac{x^*}{\lambda} \\ \pm \frac{Ry^*}{\lambda} & -1 - |f| \pm \frac{y^*}{\lambda} \end{pmatrix} \begin{pmatrix} \xi \\ \eta \end{pmatrix} \text{ iff } f \neq 0 \quad (2.32)$$

Due to the relationship between trace T , determinant D and eigenvalues of the 2×2 matrix A , we can use $T^2 - 4D$ to determine the nature of the critical point (x^*, y^*) [22]. Let us calculate the trace of A

$$\begin{aligned} T = \text{trace}(A) &= -\delta - |f| \pm \frac{Rx^*}{\lambda} - 1 - |f| \pm \frac{y^*}{\lambda} \\ &= -(\delta + 3|f| + 1) \end{aligned} \quad (2.33)$$

Given $\delta > 0$, it follows that $T < 0$ for all f . Let us calculate the determinant of A

$$\begin{aligned} D = \det(A) &= (-\delta - |f| \pm \frac{Rx^*}{\lambda})(-1 - |f| \pm \frac{y^*}{\lambda}) - (\pm \frac{x^*}{\lambda})(\pm \frac{Ry^*}{\lambda}) \\ &= (\delta + 2|f|)(1 + |f|) \pm (1 - \delta) \frac{y^*}{\lambda} \text{ iff } f \neq 0 \end{aligned} \quad (2.34)$$

When investigating stability under the condition $f < 0$, thus at the equilibrium values f_1 and f_2 , the determinant at this condition must be assessed [16]. The expression for the determinant (2.35) is decreasing for $f \in (-\infty, 0)$ and changes sign between f_1 and f_2 . Utilizing the expression for y^* , the determinant for the system when $f < 0$ can be written as

$$D = \det(A) = (\delta - 2f)(1 - f) - \frac{1 - \delta}{\lambda(1 - f)} \quad (2.35)$$

If there are two negative solutions f_1 and f_2 with $f_1 < f_2 < 0$, then $D > 0$ at f_1 , meaning that the point at the equilibrium value f_1 is a stable equilibrium [16]. At f_2 we have that $D < 0$, so the point at the equilibrium value f_2 is a saddle node. Since

$$T^2 - 4D = (1 - \delta - f)^2 - \frac{4(1 - \delta)}{\lambda(1 + f)} < 0 \quad (2.36)$$

This is true for all $f < 0$, hence the point at f_1 must be a stable node. Investigating the solution f_3 , it follows from (2.35) that when $f < 0$ then $D > 0$. Furthermore,

$$\begin{aligned} T^2 - 4D &= (\delta + 3|f| + 1)^2 - 4((\delta + 2|f|)(1 + |f|) \pm (1 - \delta) \frac{y^*}{\lambda}) \\ &= (1 - \delta - |f|)^2 - \frac{4(1 - \delta)}{\lambda} < 0 \end{aligned} \quad (2.37)$$

The equilibrium solution associated with (x_3^*, y_3^*) is a stable spiral point. These analytical results can be confirmed by a numerical approach, that is presented in Table 1, for the parameters $\lambda = \frac{1}{5}$, $R = 2$, $\delta = \frac{1}{6}$. This approach involves analyzing the placement of the eigenvalues in the complex plane (\mathbb{C}). The analysis shows that the model exhibits two stable regimes, one when $f < 0$, where temperature drives the density difference and the capillary

flow going from the cold to the warm box. The other being when $f > 0$, where salinity drives the density difference with the capillary flow going from the warm to the cold box.

Equilibrium values	(x^*, y^*) equilibrium values	Eigenvalues of A	Equilibrium type
$f_1 = -1.068$	$(0.135, 0.484)$	$-3.609, -0.761$	Stable node
$f_2 = -0.307$	$(0.352, 0.765)$	$-2.849, 0.761$	Saddle
$f_3 = 0.219$	$(0.432, 0.820)$	$-0.921 \pm 1.823i$	Stable spiral

Table 1: Equilibrium values and types. For parameters $\lambda = \frac{1}{5}$, $R = 2$, $\delta = \frac{1}{6}$. From the analysis of the eigenvalues placement in the complex plane (\mathbb{C}) it becomes evident that the equilibrium type for f_1 indeed is a stable node as $\lambda_1 < 0$ and $\lambda_2 < 0$. For f_2 it is a saddle as $\lambda_1 < 0$ and $\lambda_2 > 0$. For f_3 it is a stable spiral as $\lambda_{1,2} = a \pm bi$, where $a < 0$.

Phase Portrait

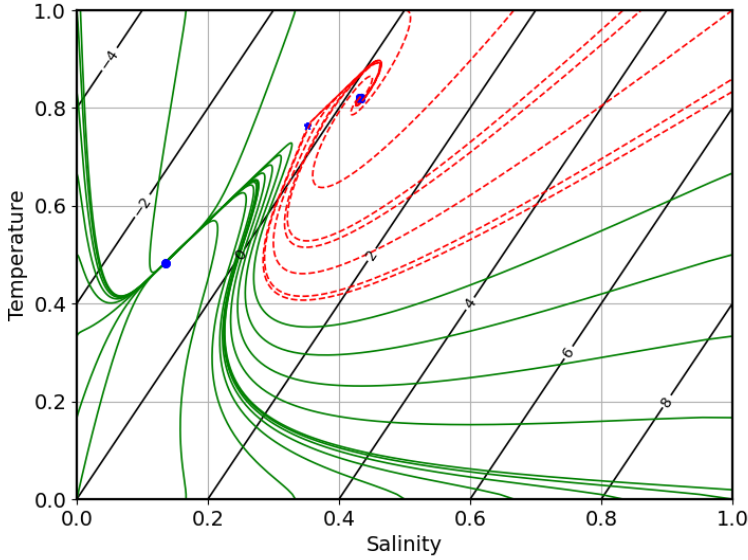


Figure 13: The xy -phase portrait for $\lambda = \frac{1}{5}$, $R = 2$, $\delta = \frac{1}{6}$. The phase portrait shows the trajectories that temperature and salinity profiles follows as they approach equilibrium points. The level sets represents the values of f . When $f > 0$ thus f is above the line $f = 0$ temperature dominates, driving the flow from the cold to the warm box. When $f < 0$ the salinity dominates, driving the flow from the warm to the cold box. The green trajectory is for the initial conditions for which the solution will reach the equilibrium at the stable node. The red trajectory is for the initial conditions for which the solution will reach the equilibrium at the stable spiral node. The saddle point lies between the two stable nodes and is repulsing the green trajectories while it is attracting the red trajectories. It is interesting to notice that there exists trajectories that cross $f = 0$, indicating the existence of initial conditions where deep water flow reverses over time.

For a further investigation of the dynamics in (2.25), the xy -phase plane is shown in Figure 13. It shows the paths which temperature and salinity follow in the course of approaching equilibrium points. Here the traverse lines indicate the values of f . Above the line $f = 0$ the flow is dominated by temperature, and is going from the cold box to the warm box. And below this line it is dominated by salinity and is going from the warm to the cold box. It is also interesting to note that there exists trajectories that cross the $f = 0$ line, this shows that there exists initial conditions for which the deep water flow slows down and then reverses over time.

Bifurcations

Any of the parameters δ , R and λ can be chosen as the bifurcation parameter in the bifurcation analysis. We choose λ as it is inversely proportional to the flow rate in (2.27), and represents factors such as bottom friction and wind driven turbulence in the mixing layer [3], making it more difficult for the water to flow from one basin to the other. As such, the flow rate decreases when λ increases. It allows us to investigate how the resistance is influencing the flow rates of the AMOC. The effects of *fresh water forcing* described by R are investigated in Appendix 5.1.5, where R is chosen as a bifurcation parameter [23]. The temperature and salinity anomalies of the surrounding boxes are kept constant, as well as the ratio of salinity and temperature exchange between the boxes and their surroundings. To investigate bifurcations exhibited by the model, it is interesting to look at the set of initial conditions, denoted S_i for which the corresponding solutions of (2.29a) converges to (x_i^*, y_i^*) as $t \rightarrow \infty$, $i = 1, 2$, called *basins of attraction* [16]. In Figure 13, there are two sets S_1 and S_2 denoted by the green and the red trajectories. The system would require a big perturbation to enable a solution close to the stable node (x_1^*, y_1^*) to jump to S_2 , causing a reversal of the flow.

In Figure 12 the red line represents λf for $\lambda = \frac{1}{3}$, and has three equilibrium flows: $f_1 < f_2 < 0 < f_3$, their stability remains unchanged from $\lambda = \frac{1}{5}$, as investigated in Section 2.3.3. The red line in Figure 12 corresponds to the left figure in Figure 14. As λ is closer to the bifurcation value $\lambda_b = 0.333$ (A.13) the stable node (x_1^*, y_1^*) and the saddle node (x_2^*, y_2^*) are closer to merging. In this case a solution closer to (x_1^*, y_1^*) would need a smaller perturbation to jump from S_1 to S_2 , resulting in a reversion of the flow.

In Figure 12, the green line represents λf for $\lambda = \frac{2}{5}$, and has only one equilibrium flow rate for $f_1 > 0$, as the stable node and the saddle node merged through a *saddle-node bifurcation* at λ_b . The flow is stuck in the state where deep water flows from warm box to the cold box, and salinity is the primary factor driving density differences.

The *bifurcation diagram* in Figure 15, shows the equilibrium flow rates f as a function of flow resistance λ , having $\delta = \frac{1}{6}$ and $R = 2$. The blue and green parts of the curve correspond to stable equilibrium for the system (2.25), while the dashed orange part corresponds to the unstable saddle point. As λ increases to the bifurcation value λ_b , the flow rate jumps to the green curve; climate scientists often use the term *tipping point* to describe such a bifurcation.

An interesting behaviour of the model can be observed when investigating at the blue curve in Figure 15. When $\lambda < \lambda_b$ and is increased towards λ_b f jumps to the stable green curve. Upon decreasing λ again f remains on the stable green curve. Here the system is

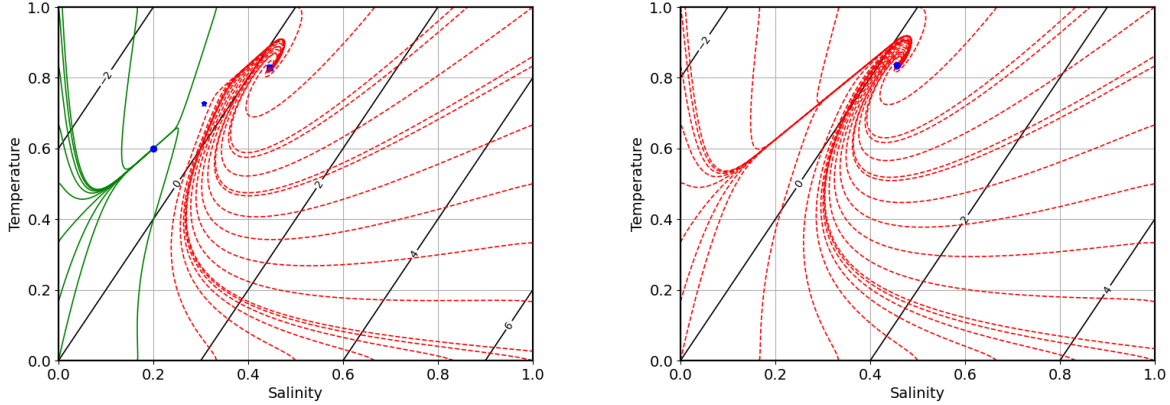


Figure 14: On the left is the phase portrait corresponding to $\lambda = \frac{1}{3}$, on the right is the phase portrait for $\lambda = \frac{2}{5}$, both sharing the parameters $R = 2$ and $\delta = \frac{1}{6}$. As λ is inversely proportional to the flow rate, the two diagrams show the evolution of the flow rates as λ increases. It can be seen that as $\lambda \rightarrow \lambda_b$ the stable node and the saddle node merge at λ_b through a saddle-node bifurcation. The bifurcation has happened in the right figure, with the stable spiral point at $f > 0$, meaning that the flow rate has been reversed

at a different stable state compared to its initial state, even though the values are identical. This exemplifies the concept of *hysteresis*. The appearance of hysteresis in the model hints towards the possibility, that if the AMOC were to slow down and switch orientation, then any future return to the current state of the AMOC may prove to be a great challenge.

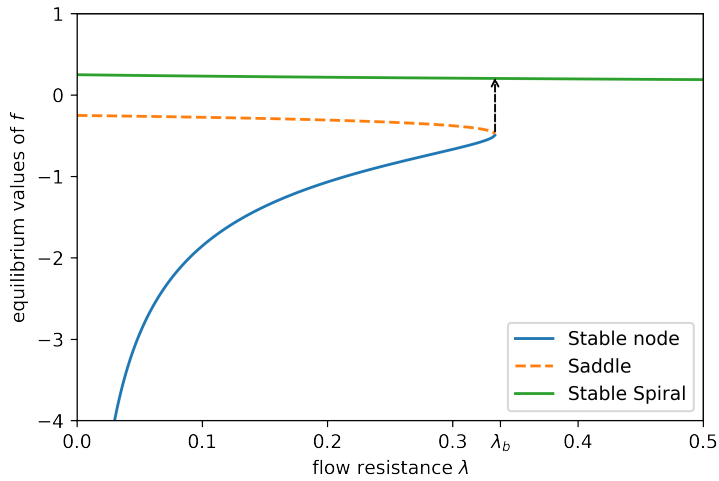


Figure 15: Bifurcation diagram for f -equilibrium values as a function of λ . Blue: stable node. Orange: Saddle node. Green: Stable spiral. The system has a saddle node bifurcation at $\lambda = \lambda_b$, where the stable node jumps to the stable spiral node. After the flow rate has jumped to the curve of the stable spiral, λ may be decreased again and f will remain on the green curve. So with the same initial conditions, the values of f are different.

3 Three Box-Model

3.1 Salinity Anomalies in the Atlantic

Salinity anomalies are events characterized by large deviations from average oceanic salinity values. Such events are known to occur in the North Atlantic and have done so on the decadal-scale with such frequency and intensity that successive salinity anomalies occurring in the 1960s, 1970s, 1980s and 1990s are collectively referred to as *Great Salinity Anomalies* (GSA) [24]. Consequences of these events can be logically deduced within the framework of the box-model by considering the effect of salinity change on Stommel's flow equation (2.18). Regarding the current AMOC configuration, an increase of salinity in the polar regions would strengthen the current flow directions, with a decrease in polar salinity weakening or potentially reversing the current configuration. This is supported by sea surface temperature measurements, suggesting that The GSA of the 1960s contributed to a reduction in strength of the AMOC [24].

These salinity anomalies are caused by either a freshwater influx, due to ice-melt, or freshwater outflux caused by severe weather conditions during harsh winters. During the 1970s, salinity anomalies were observed sequentially in different basins throughout the North Atlantic, leading to the conclusion that this was a freshening, *advection* event. The propagation was traced to its origins northeast of Iceland, a region containing the Nordic seas [26, 27]. A freshwater outflux was experienced during the 1980s GSA, which was likely caused by severe winters affecting ice-formation in the Labrador and Baffin sea [26].

In the following section we extend Stommel's box-model and apply it to the North Atlantic region. We consider the Labrador Sea and the Nordic Seas as two distinct polar boxes, due to their role as the main cold, deep-water formation sites of the North Atlantic [28]. We then regard the Equatorial Atlantic as our warm box, producing a warm northwards surface flow as shown in Figure 16.

3.2 Model Description

A natural extension to Stommel's Two Box-Model is to add a third box, as was done by Pierre Welander (1925-1996) in his 1986 paper [29, 30]. We make some adjustments to this model; where Welander was investigating the flow between the Arctic and Antarctic, we are restricting our location of interest to the North Atlantic. The model consists of three boxes:

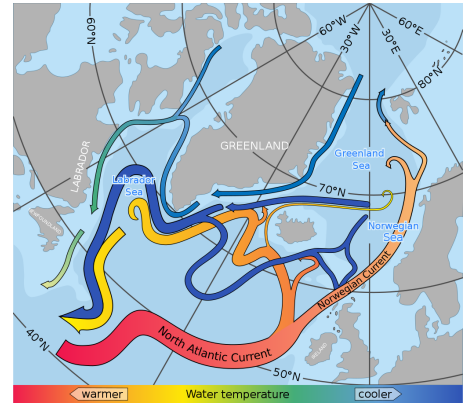


Figure 16: Currents of the North Atlantic. Cold water formation can be seen in Labrador Sea and Nordic Seas [25].

Two *cold-water* boxes, representing the two principal cold, deep-water formation sites in the North Atlantic, the Nordic seas and the Labrador sea. Additionally, there is a third box representing the warm waters of the equatorial Atlantic [31, 32]. Our primary interest will be directed toward the effect of *salinity flux* on the equilibrium states exhibited by the two overturning flows.

3.2.1 Conceptual Set-Up

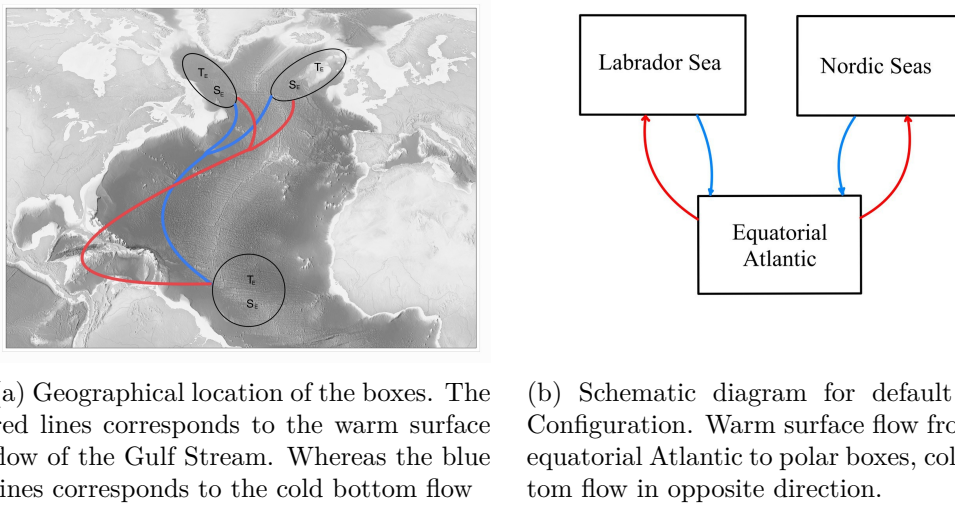


Figure 17: Conceptual setup of the three-box model.

Our model is set up with the following parameters: Three boxes, each with their own Salinity, Temperature and Salinity Flux (S, T, H respectively). The Boxes have their own boundary salinity and temperature defined by S^*, T^* . Two overturning flows q_L and q_N are present and defined as positive when the surface flow is directed northwards and bottom flow southwards.

3.2.2 System of Equations

In this section we provide an overview of the development of our system of equations. For a more comprehensive overview please refer to Appendix Section 5.2. Stommel's assumptions regarding flow rate, boundary transfer of salinity and temperature are followed, but we now treat the temperatures of each box as a fixed constant rather than a time dependent variable. This is a common modelling assumption made due to atmospheric damping effects on temperature anomalies compared with salinity anomalies [33]. We therefore assume that thermal equilibrium is reached very rapidly relative to salinity, a claim supported by both the one and two box-models and real-world climatic behaviour [4, 34, 35]. A system of equations is developed using the same process as in (2.19), with the consideration of a third box

$$\dot{S}_N = H_N + d(S_N^* - S_N) + |q_N|(S_E - S_N) \quad (3.1a)$$

$$\dot{S}_L = H_L + d(S_L^* - S_L) + |q_L|(S_E - S_L) \quad (3.1b)$$

$$\dot{S}_E = H_E + d(S_E^* - S_E) - |q_N|(S_E - S_N) - |q_L|(S_E - S_N) \quad (3.1c)$$

Where S_N , S_L and S_E represent the salinities of the two polar boxes and the equatorial Atlantic, respectively. Our equations of flow are also defined similarly to that in the two box-model (2.18)

$$q_N = k(\alpha\Delta T - \beta\Delta S_N) \quad (3.2)$$

$$q_L = k(\alpha\Delta T - \beta\Delta S_L) \quad (3.3)$$

Where $\Delta T = T_E - T_L = T_E - T_n$ and $\Delta S_L = S_E - S_L$, $\Delta S_N = S_E - S_N$. We further assume that salinity transfer between each box and its boundaries is negligible and consequently, $d \approx 0$. Moreover, we are primarily interested in the relationship between flow rate and salinity flux. Thus, we need only consider the time-dependent variation of ΔS_N and ΔS_L . We subsequently reduce our system of equations, and substitute the flow equations into the system

$$\Delta\dot{S}_N = (1 - \gamma)H - \Delta S_L|\alpha k\Delta T - \beta k\Delta S_L| - 2\Delta S_N|\alpha k\Delta T - \beta k\Delta S_N| \quad (3.4a)$$

$$\Delta\dot{S}_L = \gamma H - 2\Delta S_L|\alpha k\Delta T - \beta k\Delta S_L| - \Delta S_N|\alpha k\Delta T - \beta k\Delta S_N| \quad (3.4b)$$

Nondimensionalisation

The system is rendered dimensionless, using the following new variables representing salinity difference between the equatorial atlantic and the nordic seas: $x = \frac{\beta\Delta S_N}{\alpha\Delta T}$, salinity difference between the equatorial atlantic and labrador sea: $y = \frac{\beta\Delta S_L}{\alpha\Delta T}$ and nondimensionalised time: $\tau = \alpha k|\Delta T|t$

$$\dot{x} = (1 - \gamma)\psi - 2x|1 - x| - y|1 - y| \quad (3.5a)$$

$$\dot{y} = \gamma\psi - 2y|1 - y| - x|1 - x| \quad (3.5b)$$

Where $\psi = \frac{\beta H}{\alpha^2 k \Delta T |\Delta T|}$ is our nondimensionalised salinity flux. Note that \dot{x} and \dot{y} now refers to $\frac{d}{d\tau}$. As we will be investigating situations of symmetrical salinity flux in the two polar boxes, $\gamma = \frac{1}{2}$.

3.2.3 Equilibria and Flow Rates

Flow Rate Configurations

We regard the flow in Figure 17(b) as our default flow configuration, whereby the water in the two polar boxes is denser than the equatorial Atlantic resulting in a northwards surface flow and southwards bottom flow. There are three other possible configurations involving a reversal in either both flows or a in just one of the flows. These are visualised in Figure 24. Within our nondimensionalized system (3.5), the flow rates for the Nordic seas and Labrador

sea are represented by $1 - x$ and $1 - y$ respectively. By analysing their values at equilibrium, it is possible to make conclusions about the qualitative structural changes in both flows. Since the default configuration in 17(b) corresponds to a positive flow, a transition of $1 - x$ or $1 - y$ to a negative value, corresponds to a reversal in flow direction and subsequently a weakening or reversal of the Gulf Stream.

Negligible Salinity Flux

We conduct our first system analysis when salinity flux is set to 0 ($\psi = 0$). Equilibrium points for this system are found at $(0, 0)^T$, $(1, 0)^T$, $(0, 1)^T$, $(1, 1)^T$ and are marked in red on Figure 18. Just as in Stommel's two box-model (2.28), our absolute value terms in system (3.5) means our system has discontinuities in the second-derivatives of x and y occurring when $x = 1$ or/and $y = 1$, which physically correspond to a total shut-down in at least one of the flows. As a result of these discontinuities, it is not possible to perform a typical stability analysis via linearization and eigenvalue determination. But this is possible with $(x, y)^T = (0, 0)^T$. We again utilize the Hartman-Grobman theorem [21], and proceed to analyze the linearized system. We firstly find the Jacobian (A.26); let $f(x, y) = (\dot{x}, \dot{y})^T$ and $\nabla f(x, y)$ denote the Jacobian

$$\nabla f(x, y) = \begin{bmatrix} -2|1-x| - 2x \cdot \text{Sign}(x-1) & -|1-y| - y \cdot \text{Sign}(y-1) \\ -|1-x| - x \cdot \text{Sign}(x-1) & -2|1-y| - 2y \cdot \text{Sign}(y-1) \end{bmatrix} \quad (3.6)$$

and determine $\nabla f(0, 0)$. The eigenvalues found take the values -1 and -3 , indicating that the origin is a *stable sink*. For the remaining equilibria we resort to analysing a high resolution phase portrait shown in Figure 25, and conclude that they appear to be qualitatively similar to *saddle points*. The nature of these equilibria is coherent with reality. The equilibria with either $x = 1$ or $y = 1$ correspond to a flow shut-down. This situation would not be stable, as temperature differences would continue to drive flow, introducing new salinity differences, causing the graphical position of the solution curve to change. However, the stable sink at the origin is a possible scenario whereby all seas have reached equal salinity and flow is driven purely by temperature differences.

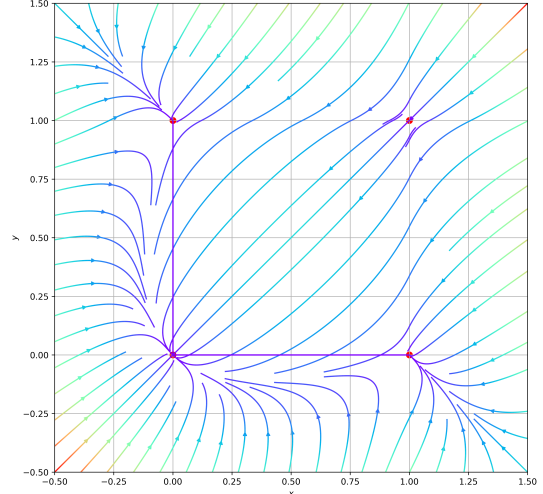


Figure 18: Phase portrait for system A.22 with 0 salinity flux ($\psi = 0$). Equilibrium points of $(0, 0)$, $(0, 1)$, $(1, 0)$, $(1, 1)$ marked in red.

Variable Salinity Flux

We now consider the effect of external salinity forcing on the system. Furthermore, we only consider the case of symmetrical salinity flux of the two polar boxes. The system of equations becomes

$$\dot{x} = \lambda - 2x|1-x| - y|1-y| \quad (3.7a)$$

$$\dot{y} = \lambda - 2y|1-y| - x|1-x| \quad (3.7b)$$

Where $\lambda = \frac{1}{2}\psi$. This will also serve as our bifurcation parameter in our subsequent analysis. Our investigation can be split into 4 phases. 1: Determining equilibria values in terms of λ . 2: Varying λ , calculating equilibria and determining their corresponding flow configurations. 3: Analysing the stability of equilibria and subsequent flow configurations for values of λ . 4: Final, comprehensive analysis on the most significant flow configurations and their relation to the Gulf Stream.

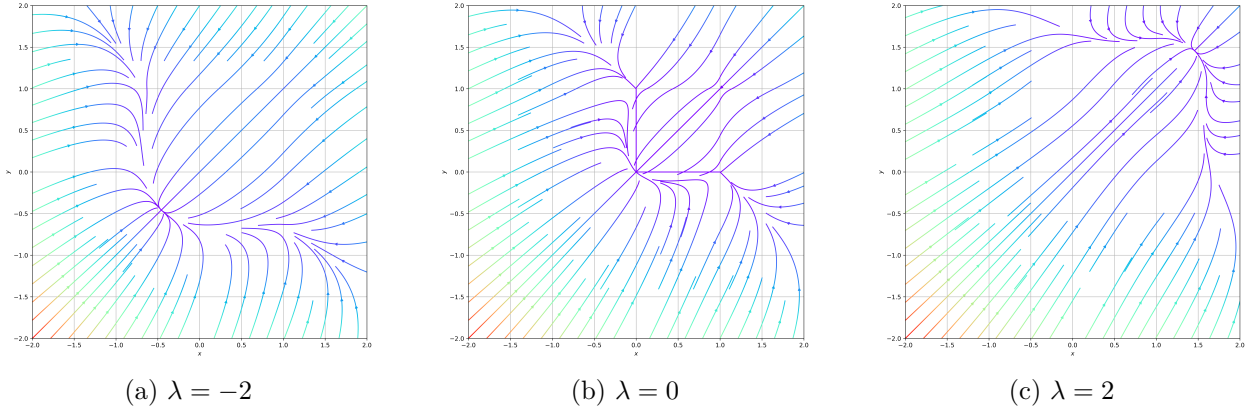


Figure 19: A sequence of phase portraits for $\lambda \in \{-2, 0, 2\}$. Qualitative changes in structure can be seen, with a sink moving in the positive x, y direction as λ increases. The symmetry of the model can also be seen, with the two phase portraits at $\lambda = \pm 2$ exhibiting a very similar topological structure.

Equilibrium points are determined, with our solution now being in terms of λ

$$\begin{aligned} \begin{bmatrix} \dot{x}^* \\ \dot{y}^* \end{bmatrix} &= \begin{bmatrix} 0 \\ 0 \end{bmatrix} \\ \begin{bmatrix} 3x^*|x^* - 1| \\ 3y^*|y^* - 1| \end{bmatrix} &= \begin{bmatrix} \lambda \\ \lambda \end{bmatrix} \end{aligned} \quad (3.8)$$

Resulting in 16 possible equilibrium values, corresponding to:

$$\begin{bmatrix} x^* \\ y^* \end{bmatrix} = \begin{bmatrix} \frac{1}{2} \pm \frac{\sqrt{9+12\lambda}}{6} \\ \frac{1}{2} \pm \frac{\sqrt{9+12\lambda}}{6} \end{bmatrix} \quad (3.9)$$

It is worth noting that complex solutions will arise for $\lambda < -\frac{3}{4}$ and $\lambda > \frac{3}{4}$ for $9 + / - 12\lambda$ respectively. No further analysis is conducted on these solutions. All possible solutions are

outlined and labelled in Appendix A.29, as well as their value for $\lambda \in \{-1, -0.5, 0.5, 1\}$ in Table 5. Much like the Stommel's two-box model, the three box-model exhibits multiple equilibrium states 5.2.2. The behaviour of these equilibria in relation to λ is investigated in the following section.

3.3 Bifurcations

The 16 different equilibrium solutions are investigated as functions of λ . In order to relate our findings to the behaviour of the Gulf Stream, we make the following observations: The surface flows presented in our model (Figure 17) arises due to the Gulf Stream. We can then consider the sum of the two flows to be representative of its overall strength. If one flow were to reverse, as in configurations 2 and 3, the effect of this on the Gulf Stream strength would be ambiguous, as the other flow could strengthen. However, if both flows were to reverse (as in configuration 4) this would correspond to a reversal in the direction of the Gulf Stream. It is therefore necessary to consider the strength and direction of the flows as a whole. The two flows are given as $1 - x$ and $1 - y$, we therefore consider the sum of the flows $Q = 2 - x - y$ as a crude measurement of the behaviour of the Gulf Stream.

Figure 20 shows the complex relationship between the sum of flow rates at equilibria and salinity flux. Symmetry is exhibited about $\lambda = 0$ and $Q = 1$. We first examine the interactions between different equilibria at the extremities of λ , beyond the critical point $\pm \frac{3}{4}$. Here, it is clear that we have multiple stable equilibria and corresponding flow configurations. The number of these can be examined via a 3D diagram as in Figure 29 or simply determined by the equilibria solutions consisting of $\sqrt{9 - 12\lambda}$ for $\lambda < -\frac{3}{4}$ and $\sqrt{9 + 12\lambda}$ for $\lambda > \frac{3}{4}$, for which there are 4 potential equilibrium states. The effect on the Gulf Stream here is somewhat ambiguous, as there exists a stable equilibrium state for each flow configuration 1, 2, 3, and 4 (see Table 7).

Turning our attention to the line $\lambda = 0$, there appears to be a very complex system of interactions between multiple equilibria, with solutions either maintaining their current stability or undergoing a switch in stability. For example, consider the equilibrium points (x_1, y_2) and (x_2, y_1) .

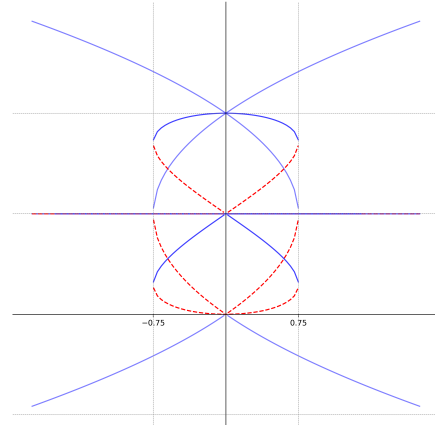


Figure 20: Bifurcation diagram for our three box-model. Blue consistent/red dashed lines represent stable and unstable equilibrium solutions respectively. Grid lines at $\lambda = \pm \frac{3}{4}$ and $Q = -1, 1, 2$. Symmetry about $x = 0$ and $2 - x - y = 1$ can clearly be seen. Please refer to 26 for a more detailed distinction of stable, unstable and saddle-point equilibria.

Their interaction at the $\lambda = 0$ is shown in more detail in the appendix 20. However, it involves the two equilibria colliding and exchanging their stabilities as λ goes from positive to negative. An analysis of nullcline interactions further highlights their complexity (see Figure 30) as it is unclear if nullclines become tangential, which would lead to a clear confirmation of the existence of saddle-node bifurcations [16].

3.4 Comparisons and Conclusion

3.4.1 Comparative Analysis

Both ours and Welander's model reveal a similar qualitative behavior, both models display a symmetry around the diagonal, have a stable sink and have very similar topological structures which can be compared in Figures 21 and 18. The idea of using a third box is not unique, and has been discussed heavily [4]. For example, a three box-model simulating North Atlantic flows was proposed by a group of researchers in May 2023 [33]. As in Welander's, it does not use salinity differences as the time-dependent parameters. Moreover, no nondimensionalization process takes place, with the model relying on real-world data and reasonable assumptions to produce suitable parameter values. In comparison, our model has a slightly different expression, but most importantly has the ability to investigate the behavior of the salinity differences and their effect on the dynamics of the Northern Atlantic from a nondimensionalized perspective. This allows us to bypass any issues related to the accuracy of experimentally determined or estimated values. Despite this, all models have very similar qualitative behaviour. After re-writing the model presented in [33] in terms of salinity differences, it too consists of 4 equilibrium points, with a single stable sink, when freshwater forcing/salinity flux is negligible.

3.4.2 Conclusion

In this work we provide a brief introduction to the dynamical systems and bifurcation theory necessary for understanding Stommel's two-box model. Stommel initially introduced this model as an idealized conceptual representation of ocean dynamics, highlighting the concept of bistability in oceanic systems [7]. Building upon Stommel's work, Welander expanded the model by incorporating an additional box, demonstrating that multiple states of flow configuration could exist across the entire Atlantic Ocean [29]. During the process of devising our own model, we encountered several difficulties as the complexity of the model grew with the amount of parameters, the nonlinear nature of our systems and finding suitable

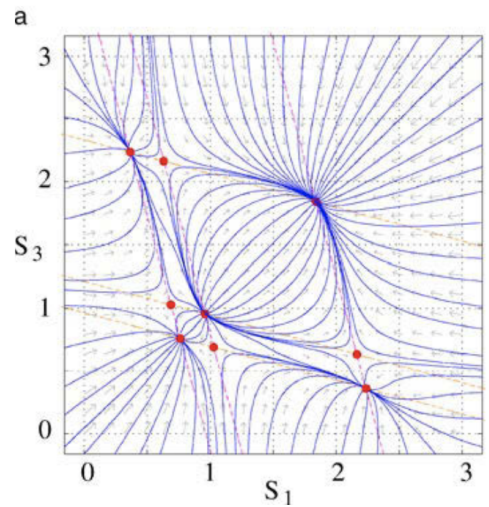


Figure 21: Phase portrait of Welander's three box model. There is a symmetry around the diagonal [4].

linear scales for nondimensionalization. This led us to simplify and make further assumptions in order to reduce parameter space and overall model complexity. The produced model gives a more simplified picture of the ocean dynamics in the Northern Atlantic. It shows that the overall orientation of the Gulf Stream may not necessarily change, even given large amounts of salinity flux.

References

- [1] IPCC, *Climate Change 2021: The Physical Science Basis. Contribution of Working Group I to the Sixth Assessment Report of the Intergovernmental Panel on Climate Change*, V. e. a. Masson-Delmotte, Ed. Cambridge, United Kingdom and New York, NY, USA: Cambridge University Press, 2021.
- [2] T. DeVries, M. Holzer, and F. Primeau, “Recent increase in oceanic carbon uptake driven by weaker upper-ocean overturning,” *Nature*, vol. 542, pp. 215–218, 2017. [Online]. Available: <https://doi.org/10.1038/nature21068>
- [3] H. Kaper and H. Engler, *Mathematics and Climate*. Society for Industrial and Applied Mathematics, 2013.
- [4] D. Olbers, J. Willebrand, and C. Eden, *Ocean Dynamics*. Berlin: Springer Verlag Berlin, May 2 2023.
- [5] K. H. Mann and J. R. N. Lazier, *Dynamics of Marine Ecosystems: Biological-Physical Interactions in the Oceans*, 3rd ed. Blackwell Publishing, 2006.
- [6] B. Qiu and R. Lukas, “Seasonal and interannual variability of the north equatorial current, the mindanao current, and the kuroshio along the pacific western boundary,” *Journal of Geophysical Research: Oceans*, vol. 101, no. C5, pp. 12 315–12 330, 1996.
- [7] H. Stommel, “Thermohaline convection with two stable regimes of flow,” *Tellus*, vol. 13, no. 2, pp. 224–230, 1961.
- [8] Noaa national centers for environmental information - world ocean atlas 2023. <https://www.ncei.noaa.gov/access/world-ocean-atlas-2023/bin/woa23.pl?parameterOption=s>. Accessed on October 18, 2023.
- [9] U.S. Geological Survey. (Year of the Webpage, e.g., 2023) Water density. Webpage. U.S. Geological Survey. Accessed on October 18, 2023. [Online]. Available: <https://www.usgs.gov/special-topics/water-science-school/science/water-density#overview>
- [10] Japan Oceanographic Data Center. (1993) Technical report on standard values of sea water. Technical Report. Intergovernmental Oceanographic Commission (IOC), United Nations Educational, Scientific, and Cultural Organization (UNESCO). Accessed on October 18, 2023. [Online]. Available: https://www.jodc.go.jp/jodcweb/info/ioc_doc/UNESCO_tech/096451mb.pdf
- [11] L. Bjørnø and M. Buckingham, “Chapter 1 - general characteristics of the underwater environment,” in *Applied Underwater Acoustics*, T. H. Neighbors and D. Bradley, Eds. Elsevier, 2017, pp. 1–84. [Online]. Available: <https://www.sciencedirect.com/science/article/pii/B9780128112403000011>
- [12] U. Nations, *Open Ocean Deep Sea*. Cambridge University Press, 2017.

- [13] NOAA, “Sea water | national oceanic and atmospheric administration,” Mar 2023. [Online]. Available: <https://www.noaa.gov/jetstream/ocean/sea-water>
- [14] P. Holmes, “Poincaré, celestial mechanics, dynamical-systems theory and “chaos”,” *Physics Reports*, vol. 193, no. 3, pp. 137–163, 1990. [Online]. Available: <https://www.sciencedirect.com/science/article/pii/037015739090012Q>
- [15] J. Thompson and J. Sieber, “The role of chaos in climate variability,” *Climate Dynamics*, vol. 31, no. 5, pp. 629–647, 2008.
- [16] S. H. Strogatz, *Nonlinear Dynamics and Chaos: With Applications to Physics, Biology, Chemistry, and Engineering*, 2nd ed. Boca Raton, FL: CRC Press, 2015.
- [17] C. Wunsch, “Henry melson stommel. 27 september 1920—17 january 1992,” *Biographical Memoirs of Fellows of the Royal Society*, vol. 43, pp. 493–502, 1997. [Online]. Available: <https://royalsocietypublishing.org/doi/abs/10.1098/rsbm.1997.0027>
- [18] H. P. Langtangen and G. K. Pedersen, *Scaling of Differential Equations*. Springer, 2016.
- [19] L. D. Talley, G. L. Pickard, W. J. Emery, and J. H. Swift, *Descriptive Physical Oceanography, An Introduction*. Academic Press, 2011.
- [20] G. Teschl, *Ordinary Differential Equations and Dynamical Systems*, ser. Graduate Studies in Mathematics. Providence, Rhode Island: American Mathematical Society, 2012, eISSN 2376-9203, ISBN 978-0-8218-8328-0, ISSN 1065-7339, Zbl 1263.34002. [Online]. Available: [URLtothePDF](#)
- [21] L. Perko, *Differential Equations and Dynamical Systems*, 3rd ed., ser. Texts in Applied Mathematics. New York, NY: Springer, 2001, page 120.
- [22] S. Sutherland, “Linearization, trace and determinant,” 2011, mAT308 Spring 2011, Stony Brook University.
- [23] J. Walsh, “The ocean and climate change: Stommel’s conceptual model,” *CODEE Journal*, vol. 12, p. Article 3, 2019. [Online]. Available: <https://scholarship.claremont.edu/codee/vol12/iss1/3>
- [24] M. Dima and G. Lohmann, “Causes and consequences of the late 1960s great salinity anomaly,” in *Planet Earth 2011*, E. G. Carayannis, Ed. Rijeka: IntechOpen, 2011, ch. 10. [Online]. Available: <https://doi.org/10.5772/24820>
- [25] S. Thaarup, M. Djurhuus Poulsen, K. Thorsøe, and J. Keiding, “Study on arctic mining in greenland,” *VIDENCENTER FOR MINERALSKE RÅSTOFFER OG MATERIALE*, 11 2020.

- [26] R. R. Dickson, J. Meincke, S.-A. Malmberg, and A. J. Lee, “The “great salinity anomaly” in the northern north atlantic 1968–1982,” *Progress in Oceanography*, vol. 20, no. 2, pp. 103–151, 1988. [Online]. Available: <https://www.sciencedirect.com/science/article/pii/0079661188900493>
- [27] I. M. Belkin, S. Levitus, J. Antonov, and S.-A. Malmberg, ““great salinity anomalies” in the north atlantic,” *Progress in Oceanography*, vol. 41, no. 1, pp. 1–68, 1998. [Online]. Available: <https://www.sciencedirect.com/science/article/pii/S0079661198000159>
- [28] A. Pohl, A. Ridgwell, R. Stockey, C. Thomazo, A. Keane, E. Vennin, and C. Scotese, “Continental configuration controls ocean oxygenation during the phanerozoic,” *Nature*, vol. 608, pp. 523–527, 08 2022.
- [29] P. Welander, “Thermohaline effects in the ocean circulation and related simple models,” *journal name*, 1986. [Online]. Available: <https://api.semanticscholar.org/CorpusID:140639059>
- [30] G. Walin, “Pierre welander 1925—1996,” *Tellus A*, vol. 49, no. 1, 1997. [Online]. Available: <https://www.tandfonline.com/doi/pdf/10.3402/tellusa.v49i1.12208>
- [31] J.-E. Park, H.-C. Kim, and K.-H. Cho, “Variability of near-surface salinity in the nordic seas over the past three decades (1991-2019),” *Frontiers in Marine Science*, vol. 9, 2022. [Online]. Available: <https://www.frontiersin.org/articles/10.3389/fmars.2022.969159>
- [32] J. Zhang, W. Weijer, M. Steele *et al.*, “Labrador sea freshening linked to beaufort gyre freshwater release,” *Nature Communications*, vol. 12, p. 1229, 2021. [Online]. Available: <https://doi.org/10.1038/s41467-021-21470-3>
- [33] A. Neff, A. Keane, H. A. Dijkstra, and B. Krauskopf, “Bifurcation analysis of a north atlantic ocean box model with two deep-water formation sites,” *Journal Name (if applicable)*, May 2023.
- [34] H. Alkhayouon, P. Ashwin, L. C. Jackson, C. Quinn, and R. A. Wood, “Basin bifurcations, oscillatory instability, and rate-induced thresholds for atlantic meridional overturning circulation in a global oceanic box model,” *Proceedings of the Royal Society A*, vol. 475, no. 2225, 2019.
- [35] S. Titz, T. Kuhlbrodt, S. Rahmstorf, and U. Feudel, “On freshwater-dependent bifurcations in box models of the interhemispheric thermohaline circulation,” *Tellus A*, 01 2002.

Glossary

abyssal zone The deepest part of the ocean, extending from below the thermocline to the seafloor. It is characterized by low temperatures. 2, 3

advection Refers to the transport of heat and mass in a fluid. 21

AMOC The Atlantic meridional overturning circulation is part of a global thermohaline circulation. 1–3, 6, 11, 14, 19, 20

anomaly Refers to deviations or variations from an expected value. 8–10, 13

basins of attraction Regions in the phase space where trajectories converge towards a specific equilibrium point or a set of points. 19

flow of a system Refers to the movement of elements within a system. 4

fresh water forcing The introduction or removal of freshwater in a specific region, it affects the density and the salinity of the water. 19

Gulf Stream A warm ocean current that starts in the Gulf of Mexico, it flows along the eastern coast of North America, and heads across the Atlantic Ocean. 11, 22, 24, 25

Hartman-Grobman theorem States that the linearized system about a critical point is a sufficient approximation of the qualitative structure of the nonlinear system. 16, 24

hyperbolic equilibrium point a hyperbolic equilibrium point is an equilibrium point characterized by the eigenvalues of the Jacobian matrix having non-zero real parts. 16

hysteresis The dependence of the state of a system on its history. 20

Jacobian A matrix of consisting of the partial derivatives of functions that describes the rate of change of the function with respect to the input variables. 17, 24

level sets Used to represent and analyze the shape and boundaries of objects. 8, 9

mixing layer The section of the ocean extending to only 5 – 10m below the surface, where turbulence and sunlight maintain a relatively constant temperature. 2, 3

nondimensionalizing A process where physical quantities are scaled to remove their units, making them dimensionless. 6

phase space A space representing all possible states of a dynamical system. 3

practical salinity units Is a unit of measurement representing the salinity of seawater. 3

THC Thermohaline circulation is a part of the ocean circulation that is driven by density gradients created by surface heat and freshwater fluxes. 1, 2

thermocline The layer between the mixing layer and the abyssal zone. It is characterized by a linear decrease in temperature and extends to a depth of $\approx 1\text{km}$. 2, 3

virtual salt flux A concept that represents the salt transport without removing salt. It is equivalent to virtual fresh water flux. 12–14

4 Parameters

4.1 General parameters

Quantity	Symbol	Value and units
Hydraulic Constant	k	s^{-1}
Temperature	T	$^{\circ}C$
Boundary temperature	T^*	$^{\circ}C$
Salinity	S	psu
Boundary salinitie	S^*	psu
Flow rate	r	s^{-1}
Density	ρ	g/cm^3
Reference density	ρ_0	g/cm^3
Temperature transfer coefficient	c	s^{-1}
Salinity transfer coefficient	d	s^{-1}
Average value for thermal contraction coefficient	α	$^{\circ}C^{-1}$
Average value for saline contraction coefficient β	β	psu^{-1}
Salinity flux	H	$psu \cdot s^{-1}$

Table 2: Table of parameters

4.2 Nondimensional parameters two box model

Quantity	Symbol	Value
Temperature	y	
Salinity	x	
Flow resistance	λ	$\frac{1}{5}$
Flow rate	f	
Salinity-temperature density effect ratio	R	2
Density anomaly	σ	
Salinity-temperature equilibrium rate ratio	δ	$\frac{1}{6}$
Rescaled time	τ	

Table 3: Table of nondimensional parameters for two box model

4.3 Nondimensional parameters three box model

Quantity	Symbol	Value
Salinity difference between equatorial atlantic and labrador sea	y	
Salinity difference between equatorial atlantic and nordic seas	x	
Salinity flux	ψ	
Degree of asymmetry between labrador sea and nordic seas	γ	
Salinity flux to labrador sea and nordic seas	λ	
Salinity-temperature density effect ratio	R	2
Density anomaly	σ	
Salinity-temperature equilibrium rate ratio	δ	$\frac{1}{6}$
Rescaled time	τ	

Table 4: Table of nondimensional parameters for three box model

5 Appendix

5.1 Two Box Model

5.1.1 Two Box Nondimensionalization

In this the steps for achieving the non-dimensional system obtained in is (2.25) shown:

Temperature

$$\begin{aligned}
 \frac{d}{d\tau}(x) &= \frac{d}{dt} \left(\frac{S}{S^*} \right) \cdot \frac{d}{d\tau}(t) \\
 &= \frac{d \cdot (S^* - S) - 2 \cdot |q| \cdot S}{S^*} \cdot \frac{1}{c} \\
 &= \frac{d}{c} \cdot (1 - x) - \frac{2 \cdot |q|}{c} \cdot x \\
 &= \delta \cdot (1 - x) - |f| \cdot x
 \end{aligned} \tag{A.1}$$

Salinity equation

$$\begin{aligned}
 \frac{d}{d\tau}(y) &= \frac{d}{dt} \left(\frac{T}{T^*} \right) \cdot \frac{d}{d\tau}(t) \\
 &= \frac{c \cdot (T^* - T) - 2 \cdot |q| \cdot T}{T^*} \cdot \frac{1}{c} \\
 &= 1 - y - \frac{2 \cdot |q|}{c} \cdot y = 1 - y - |f| \cdot y
 \end{aligned} \tag{A.2}$$

5.1.2 Lipschitz Continuity

In this the steps for proving Lipschitz continuity is shown, based on Page 71, definition 2 of [21]: A function $f : E \rightarrow \mathbb{R}^n$ is said to satisfy the *Lipschitz condition* on E if there is a positive constant K , such that for all $x, y \in E$:

$$|f(x) - f(y)| \leq K|x - y| \quad (\text{A.3})$$

If f satisfies the Lipschitz condition, it is *Lipschitz continuous* in E . A crucial condition for ensuring the *existence* and *uniqueness* of solutions to differential equations [20].

Temperature equation

Let $x, y \in \mathbb{R}$. Using euclidean norm.

$$\begin{aligned} |f(x) - f(y)| &= |1 - x - |f|x - 1 + y + |f|y| \\ \Rightarrow |f(x) - f(y)| &= |y - x - |f|x + |f|y| \\ \Rightarrow |f(x) - f(y)| &= |(-1 - |f|)x - y(-1 - |f|)| \\ \Rightarrow |f(x) - f(y)| &= |(-1 - |f|)(x - y)| \\ \Rightarrow |f(x) - f(y)| &= (1 + |f|)|x - y| \leq K|x - y| \end{aligned} \quad (\text{A.4})$$

Satisfies the Lipschitz condition with any $K \in \mathbb{R} > 1 + |f|$

Salinity equation

Let $x, y \in \mathbb{R}$. Using euclidean norm.

$$\begin{aligned} |f(x) - f(y)| &= |\delta(1 - x) - |f|x - \delta(1 - y) + |f|y| \\ \Rightarrow |f(x) - f(y)| &= |\delta - \delta x - \delta + \delta y - |f|x + |f|y| \\ \Rightarrow |f(x) - f(y)| &= |-\delta x + \delta y - |f|x + |f|y| \\ \Rightarrow |f(x) - f(y)| &= |-\delta(x - y) - |f|(x - y)| \\ \Rightarrow |f(x) - f(y)| &= (\delta + |f|)|x - y| \leq K|x - y| \end{aligned} \quad (\text{A.5})$$

Satisfies the Lipschitz condition with any $K \in \mathbb{R} > |\delta| + |f|$

5.1.3 Solutions to system

We have

$$\lambda f = Rx^* - y^* = \frac{R\delta}{\delta + |f|} - \frac{1}{1 + |f|} \quad (\text{A.6})$$

Let $\delta = \frac{1}{6}$, $R = 2$, $\lambda = \frac{1}{5}$.

$$\frac{1}{5}f = \frac{\frac{1}{3}}{\frac{1}{6} + |f|} - \frac{1}{1 + |f|} \quad (\text{A.7})$$

Let $f < 0$.

$$\frac{f}{5} = \frac{1 + 4f}{6f^2 - 7f + 1} \Rightarrow f = \{-1.068, -0.308\} \quad (\text{A.8})$$

Let $f > 0$

$$\frac{f}{5} = \frac{1 - 4f}{6f^2 + 7f + 1} \Rightarrow f = 0.219 \quad (\text{A.9})$$

5.1.4 Bifurcation value

In this the steps for finding the bifurcation value is shown.

Finding λ_b

Let $R = 2$ and $\delta = \frac{1}{6}$ and assuming $f < 0$. Meaning that the the bifurcation is expected to happen before the flow changes direction.

$$\lambda f = \frac{1 + 4f}{6f^2 - 7f + 1} \Rightarrow \quad (\text{A.10})$$

$$f_1 = -\frac{\left(\left(154\lambda + 1242 + 9\sqrt{-\frac{3(25\lambda^3 - 720\lambda^2 - 4364\lambda + 1536)}{\lambda}}\right)\lambda^2\right)^{\frac{1}{3}}}{36\lambda} - \frac{31\lambda + 72}{36\left(\left(154\lambda + 1242 + 9\sqrt{-\frac{3(25\lambda^3 - 720\lambda^2 - 4364\lambda + 1536)}{\lambda}}\right)\lambda^2\right)^{\frac{1}{3}}} + \frac{7}{18} \\ + \frac{I\sqrt{3}\left(\frac{\left(\left(154\lambda + 1242 + 9\sqrt{-\frac{3(25\lambda^3 - 720\lambda^2 - 4364\lambda + 1536)}{\lambda}}\right)\lambda^2\right)^{\frac{1}{3}}}{18\lambda} - \frac{31\lambda + 72}{18\left(\left(154\lambda + 1242 + 9\sqrt{-\frac{3(25\lambda^3 - 720\lambda^2 - 4364\lambda + 1536)}{\lambda}}\right)\lambda^2\right)^{\frac{1}{3}}}\right)}{2} \quad (\text{A.11})$$

$$f_2 = -\frac{\left(\left(154\lambda + 1242 + 9\sqrt{-\frac{3(25\lambda^3 - 720\lambda^2 - 4364\lambda + 1536)}{\lambda}}\right)\lambda^2\right)^{\frac{1}{3}}}{36\lambda} - \frac{31\lambda + 72}{36\left(\left(154\lambda + 1242 + 9\sqrt{-\frac{3(25\lambda^3 - 720\lambda^2 - 4364\lambda + 1536)}{\lambda}}\right)\lambda^2\right)^{\frac{1}{3}}} + \frac{7}{18} - \\ \frac{I\sqrt{3}\left(\frac{\left(\left(154\lambda + 1242 + 9\sqrt{-\frac{3(25\lambda^3 - 720\lambda^2 - 4364\lambda + 1536)}{\lambda}}\right)\lambda^2\right)^{\frac{1}{3}}}{18\lambda} - \frac{31\lambda + 72}{18\left(\left(154\lambda + 1242 + 9\sqrt{-\frac{3(25\lambda^3 - 720\lambda^2 - 4364\lambda + 1536)}{\lambda}}\right)\lambda^2\right)^{\frac{1}{3}}}\right)}{2} \quad (\text{A.12})$$

This yields the solution of λ_b :

$$f_1 = f_2 \Rightarrow \lambda_b = 0.333 \quad (\text{A.13})$$

5.1.5 Using R as bifurcation parameter

Using R as a bifurcation parameter corresponds to investigating the effects of freshwater forcing. This assumes that the capillary flow is from the cold to the warm box, then removing an amount of water is removed from the cold box, which is then being replaced by a cold, salt free amount of the same volume. Recalling that $R > 1$, with $R = \frac{\beta S^*}{\alpha T^*}$ measures the relative effects of salinity and temperature on density, the reduced salt content will lead to lower density in the cold box and therefore a weaker circulation.

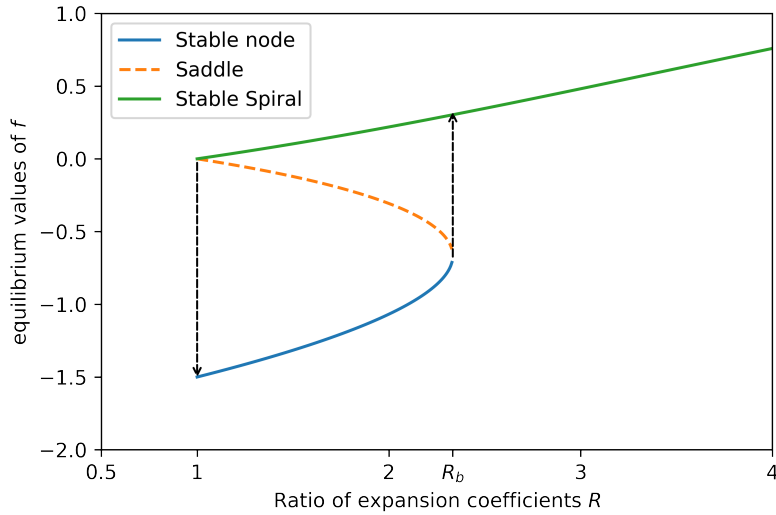


Figure 22: Bifurcation diagram for f -equilibrium values as a function of R , with $\lambda = \frac{1}{5}$, $\delta = \frac{1}{6}$, $R = \frac{\beta S^*}{\alpha T^*}$ and $R > 1$. Having R as a bifurcation parameter, corresponds to investigating the effects of freshwater forcing into the system. Assuming constant volume. The bifurcation diagram is plotted for $R \in (1, 4)$ to show the hysteresis associated with the bifurcation diagram. The hysteresis can be seen when $R \rightarrow 1$ while R is on the green curve, here R jumps from green curve of the stable spiral curve to the blue curve of the stable node.

5.2 Three Box-Model

5.2.1 Derivation

Initial System

Same assumptions as in Stommel's two-box model. However, we assume negligible salinity transfer between oceanic boundaries (i.e., $d = 0$), that the two polar boxes have equal temperature and that all temperatures are considered constant. We also include a non-zero salinity flux H into the equatorial Atlantic. Due to conservation of salinity, an equal amount of salinity outflux must be experienced by the two polar boxes. The variable γ represents the proportion of this salinity flux handled by the Nordic seas, whereas $(1 - \gamma)$ is the proportion experienced by the Labrador sea.

Time-dependent Salinity:

Nordic Seas:

$$\frac{d}{dt}(S_N) = \gamma \cdot H + |q_N|(\Delta S_N) \quad (\text{A.14})$$

Labrador Sea:

$$\frac{d}{dt}(S_L) = (1 - \gamma) \cdot H + |q_L|(\Delta S_L) \quad (\text{A.15})$$

Equatorial Atlantic:

$$\frac{d}{dt}(S_E) = H - |q_L|(\Delta S_L) - |q_N|(\Delta S_N) \quad (\text{A.16})$$

Where $\Delta S_L = S_E - S_L$, $\Delta S_N = S_E - S_N$ and that ΔT is constant.

Flow equations:

Nordic Sea Flow:

$$\begin{aligned} q_N &= k \cdot \frac{\rho_N - \rho_E}{\rho_0} \\ &= k \cdot (1 - \alpha T_N + \beta S_N) - k(1 - \alpha T_E + \beta S_E) \\ &= \alpha k(\Delta T) - \beta k(\Delta S_N) \end{aligned} \quad (\text{A.17})$$

Labrador Sea Flow:

$$\begin{aligned} q_L &= k \frac{\rho_L - \rho_E}{\rho_0} \\ &= (1 - \alpha T_L + \beta S_L) - (1 - \alpha T_E + \beta S_E) \\ &= \alpha k(\Delta T) - \beta k(\Delta S_L) \end{aligned} \quad (\text{A.18})$$

Reduction to Two-Dimensions

By considering the ΔS_N and ΔS_L as our new time-dependent variables of interest, we are able to reduce this system to 2 Dimensions

$$\begin{aligned} \frac{d}{dt}(\Delta S_N) &= \frac{d}{dt}(S_E) - \frac{d}{dt}(S_N) \\ &= (H - |q_L|(\Delta S_L) - |q_N|(\Delta S_N)) - (\gamma H + |q_N|(\Delta S_N)) \\ &= (1 - \gamma)H - |q_L|(\Delta S_L) - 2 \cdot |q_N|(\Delta S_N) \end{aligned} \quad (\text{A.19})$$

$$\begin{aligned} \frac{d}{dt}(\Delta S_L) &= \frac{d}{dt}(S_E) - \frac{d}{dt}(S_L) \\ &= (H - |q_L|(\Delta S_L) - |q_N|(\Delta S_N)) - ((1 - \gamma)H + |q_L|(\Delta S_L)) \\ &= \gamma H - 2|q_L|(\Delta S_L) - |q_N|(\Delta S_N) \end{aligned} \quad (\text{A.20})$$

Substituting flow equations with time-dependent variables into system of equations

$$\frac{d}{dt} (\Delta S_N) = (1 - \gamma) H - |\alpha k (\Delta T) - \beta k (\Delta S_L)| (\Delta S_L) - 2|\alpha k (\Delta T) - \beta k (\Delta S_N)| (\Delta S_N) \quad (\text{A.21a})$$

$$\frac{d}{dt} (\Delta S_L) = \gamma H - 2|\alpha k (\Delta T) - \beta k (\Delta S_L)| (\Delta S_L) - |\alpha k (\Delta T) - \beta k (\Delta S_N)| (\Delta S_N) \quad (\text{A.21b})$$

Nondimensionsalisation

Nondimensionalising, using the following linear scales: $x = \frac{\beta \Delta S_N}{\alpha \Delta T}$, $y = \frac{\beta \Delta S_L}{\alpha \Delta T}$, $\tau = \alpha k |\Delta T| t$

$$\begin{aligned} \frac{d}{d\tau} (x) &= \frac{d}{dt} \left(\frac{\beta \Delta S_N}{\alpha \cdot \Delta T} \right) \frac{d}{d\tau} (t) \\ &= \frac{\beta}{\alpha \Delta T} \frac{d}{dt} (\Delta S_N) \frac{1}{\alpha k |\Delta T|} \\ &= \vdots \\ &= (1 - \gamma) \psi - |1 - y|y - 2|1 - x|x \end{aligned} \quad (\text{A.22})$$

$$\begin{aligned} \frac{d}{d\tau} (y) &= \frac{d}{dt} \left(\frac{\beta \Delta S_L}{\alpha \Delta T} \right) \frac{d}{d\tau} (t) \\ &= \frac{\beta}{\alpha \Delta T} \frac{d}{dt} (\Delta S_L) \frac{1}{\alpha k |\Delta T|} \\ &= \vdots \\ &= \gamma \psi - 2|1 - y|y - |1 - x|x \end{aligned} \quad (\text{A.23})$$

Where $\psi = \frac{\beta H}{\alpha^2 k \Delta T |\Delta T|}$. Due to the assumption of symmetrical salinity flux, the system is further reduced to

$$\dot{x} = \lambda - |1 - y|y - 2|1 - x|x \quad (\text{A.24a})$$

$$\dot{y} = \lambda - 2|1 - y|y - |1 - x|x \quad (\text{A.24b})$$

Where $\lambda = \frac{1}{2}\psi$.

5.2.2 Symmetrical Salinity Flux

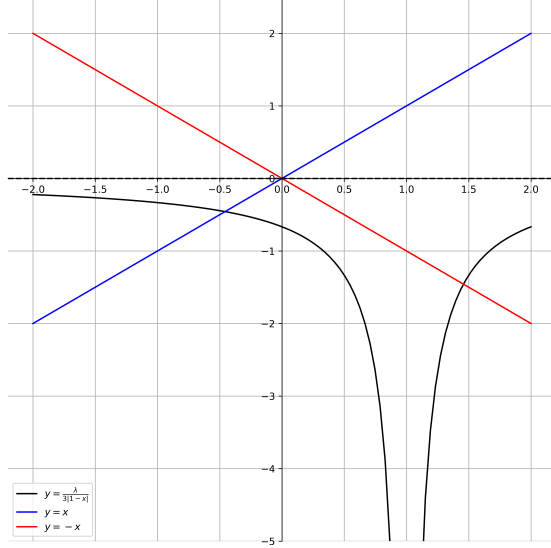
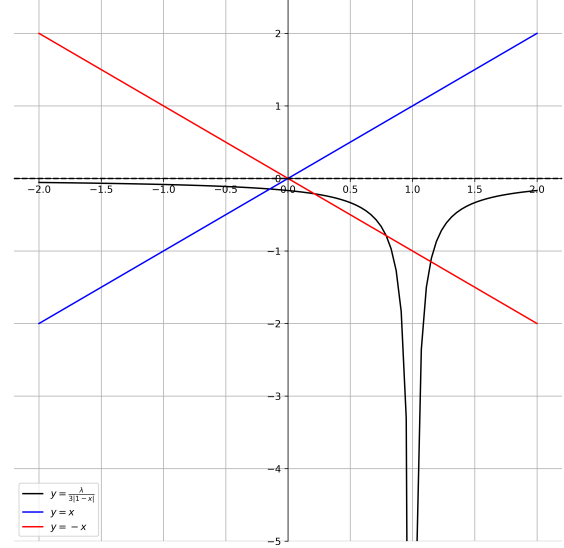
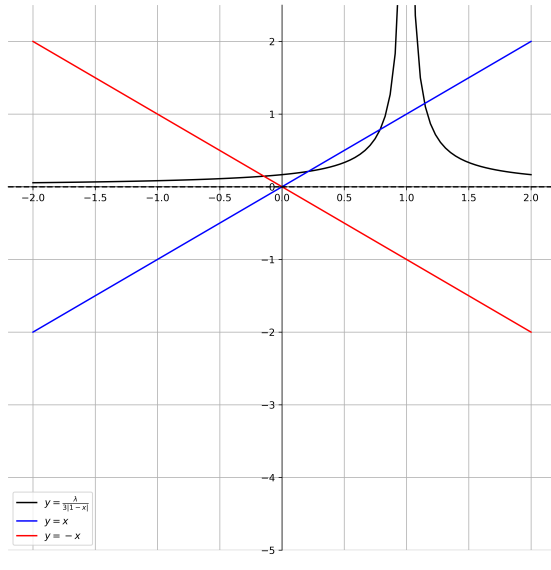
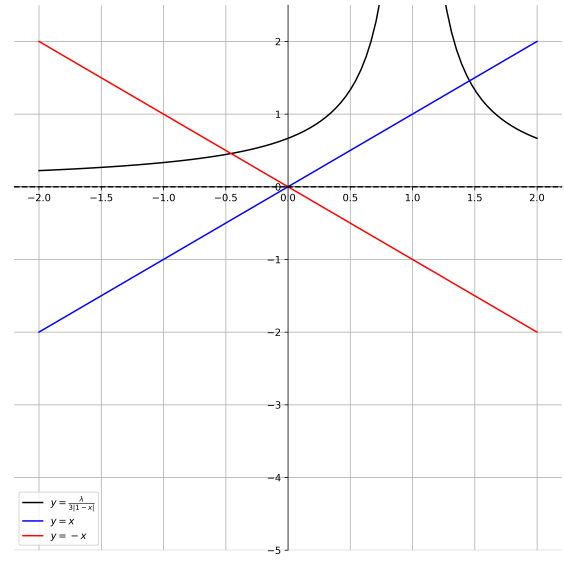
Finding Equilibria

Re-writing system (A.24) in matrix form

$$\begin{aligned}
 & \begin{bmatrix} 2 \cdot |1-x| & |1-y| \\ |1-x| & 2 \cdot |1-y| \end{bmatrix} \begin{bmatrix} x \\ y \end{bmatrix} = \begin{bmatrix} \lambda \\ \lambda \end{bmatrix} \\
 \Rightarrow & \begin{bmatrix} x \\ y \end{bmatrix} = \begin{bmatrix} \frac{2}{3|x-1|} & -\frac{1}{3|x-1|} \\ -\frac{1}{3|y-1|} & \frac{2}{3|y-1|} \end{bmatrix} \begin{bmatrix} \lambda \\ \lambda \end{bmatrix} \\
 \Rightarrow & \begin{bmatrix} x \\ y \end{bmatrix} = \begin{bmatrix} \frac{\lambda}{3|x-1|} \\ \frac{\lambda}{3|y-1|} \end{bmatrix}
 \end{aligned} \tag{A.25}$$

Solving produces $\frac{1}{2} \pm \frac{\sqrt{9+12\lambda}}{6}$ for both x and y .

Number of Equilibria as $|\lambda|$ Increases

(a) $\lambda = -2$ (b) $\lambda = -\frac{1}{2}$ (c) $\lambda = \frac{1}{2}$ (d) $\lambda = 2$ Figure 23: Number of real equilibrium solutions for three box-model decreases as $|\lambda|$ increases.

Determining Jacobian

Let $f_1(x, y) = \dot{x}$ and $f_2(x, y) = \dot{y}$

$$\begin{aligned}\nabla f(x, y) &= \begin{pmatrix} \frac{\partial f_1}{\partial x}(x, y) & \frac{\partial f_1}{\partial y}(x, y) \\ \frac{\partial f_2}{\partial x}(x, y) & \frac{\partial f_2}{\partial y}(x, y) \end{pmatrix} \\ &= \begin{pmatrix} -2|1-x| - 2x\text{Sign}(x-1) & -|1-y| - y\text{Sign}(y-1) \\ -|1-x| - x\text{Sign}(x-1) & -2|1-y| - 2y\text{Sign}(y-1) \end{pmatrix}\end{aligned}\quad (\text{A.26})$$

5.2.3 Flow Configurations

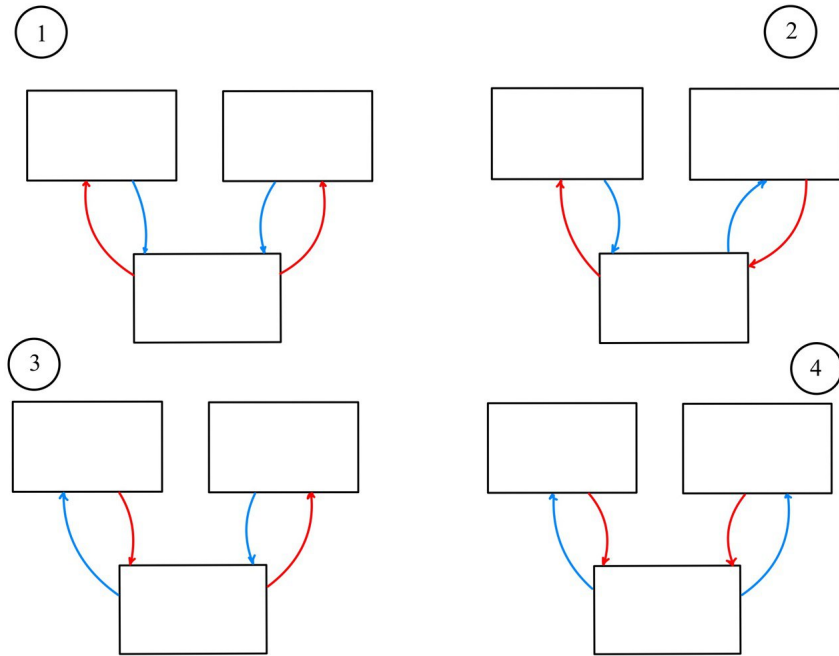


Figure 24: Possible Flow Configurations. Red represents surface flow, blue bottom flow. 1 represents the default configuration of northwards surface flow, southwards bottom flow. 2 represents a reversal in the Nordic flow. 3 is a reversal in the Labrador flow. and 4 a reversal of both flows.

5.2.4 Interpreting Nondimensionalized Flows

Flow Rates during nondimensionalization:
Nordic Sea Flow

$$\frac{\beta}{\alpha^2 \cdot \Delta T \cdot k \cdot |\Delta T|} \cdot (\alpha \cdot k \cdot \Delta T - \beta \cdot k \cdot \Delta S_N) = \dots = 1 - x \quad (\text{A.27})$$

Labrador Sea Flow

$$\frac{\beta}{\alpha^2 \cdot \Delta T \cdot k \cdot |\Delta T|} (\alpha \cdot k \cdot (\Delta T) - \beta \cdot k \cdot \Delta S_L) = \dots = 1 - y \quad (\text{A.28})$$

Sum of both flows is $q_L + q_N$, nondimensionalized as $(1 - x) + (1 - y) = 2 - (x + y)$. Thus, the behaviour of the two flows can be determined via the sign of $2 - x - y$.

- $2 - x - y < 0 \Rightarrow$ Reversal of both flows. Gulf Stream reversed.
- $2 - x - y = 0 \Rightarrow$ Shutdown of both flows. Gulf Stream shutdown.
- $2 - x - y > 0 \Rightarrow$ Increase in flow strength. Gulf Stream strengthened.

It is also true that if either $1 - x$ or $1 - y$ becomes negative, the gulf stream will weaken.

5.2.5 Equilibria and Stability Analysis

We define the following equilibrium points with respect to λ . The analysis is conducted to analyse the stability of the equilibrium points. First we define the equilibrium points.

$$\begin{aligned} x_1 &= \frac{1}{2} - \frac{\sqrt{9 + 12\lambda}}{6}, x_2 = \frac{1}{2} - \frac{\sqrt{9 - 12\lambda}}{6} \\ x_3 &= \frac{1}{2} + \frac{\sqrt{9 - 12\lambda}}{6}, x_4 = \frac{1}{2} + \frac{\sqrt{9 + 12\lambda}}{6} \\ y_1 &= \frac{1}{2} + \frac{\sqrt{9 + 12\lambda}}{6}, y_2 = \frac{1}{2} + \frac{\sqrt{9 - 12\lambda}}{6} \\ y_3 &= \frac{1}{2} - \frac{\sqrt{9 + 12\lambda}}{6}, y_4 = \frac{1}{2} - \frac{\sqrt{9 - 12\lambda}}{6} \end{aligned} \quad (\text{A.29})$$

The following tables contain various values relating to the equilibria solutions. Please note that equilibrium values of x and y have been omitted for values of λ where complex values have been encountered.

Equilibrium	λ			
	-1	-0.5	0.5	1
(x_1, y_1)		(0.211, 0.789)	(-0.145, 1.145)	(-0.264, 1.264)
(x_1, y_2)		(0.211, 1.145)	(-0.145, 0.789)	
(x_1, y_3)		(0.211, 0.211)	(0.145, -0.145)	(-0.264, -0.264)
(x_1, y_4)		(0.211, -0.145)	(-0.145, 0.211)	
(x_2, y_1)		(-0.145, 0.789)	(0.211, 1.145)	
(x_2, y_2)	(-0.264, 1.264)	(-0.145, 1.145)	(0.211, 0.789)	
(x_2, y_3)		(-0.145, 0.211)	(0.211, -0.145)	
(x_2, y_4)	(-0.264, 0.264)	(-0.145, -0.145)	(0.211, 0.211)	
(x_3, y_1)		(1.145, 0.789)	(0.789, 1.145)	
(x_3, y_2)	(1.264, 1.264)	(1.145, 1.145)	(0.789, 0.789)	
(x_3, y_3)		(1.145, 0.211)	(0.789, -0.145)	
(x_3, y_4)	(1.264, -0.264)	(1.145, -0.145)	(0.789, 0.211)	
(x_4, y_1)		(0.789, 0.789)	(1.145, 1.145)	(1.264, 1.264)
(x_4, y_2)		(0.789, 1.145)	(1.145, 0.789)	
(x_4, y_3)		(0.789, 0.211)	(1.145, -0.145)	(1.264, -0.264)
(x_4, y_4)		(0.789, -0.145)	(1.145, 0.211)	

Table 5: Equilibrium values for varying values of λ .

Equilibrium	Eigenvalues and λ				Stability
	-1	-0.5	0.5	1	
(x_1, y_1)		-0.99, 0.99	-3.87, -1.29	$\frac{-\sqrt{21}}{3}, -\sqrt{21}$	Saddle \rightarrow Sink
(x_1, y_2)		-0.75, -2.98	-2.37, 0.94		Sink \rightarrow Saddle
(x_1, y_3)		-0.58, -1.73	-1.29, -3.87	$\frac{-\sqrt{21}}{3}, -\sqrt{21}$	Sink
(x_1, y_4)		-0.75, -2.98	-2.89, -0.75		Sink
(x_2, y_1)		-2.37, 0.94	-0.75, -2.98		Saddle \rightarrow Sink
(x_2, y_2)	$\frac{-\sqrt{21}}{3}, -\sqrt{21}$	-3.87, -1.29	-0.99, 0.99		Sink \rightarrow Saddle
(x_2, y_3)		-2.98, -0.75	-0.75, -2.98		Sink
(x_2, y_4)	$\frac{-\sqrt{21}}{3}, -\sqrt{21}$	-1.29, -3.87	-0.57, -1.73		Sink
(x_3, y_1)		-2.37, 0.94	0.94, -2.37		Saddle
(x_3, y_2)	$\frac{-\sqrt{21}}{3}, -\sqrt{21}$	-1.29, -3.87	1.73, 0.58		Saddle \rightarrow Source
(x_3, y_3)		-2.98, -0.75	0.94, -2.37		Sink \rightarrow Saddle
(x_3, y_4)	$\frac{-\sqrt{21}}{3}, -\sqrt{21}$	-1.29, -3.87	0.99, -0.99		Sink \rightarrow Saddle
(x_4, y_1)		1.73, 0.58	-1.29, -3.87	$\frac{-\sqrt{21}}{3}, -\sqrt{21}$	Source \rightarrow Sink
(x_4, y_2)		-0.94, -2.37	-2.37, 0.94		Sink \rightarrow Saddle
(x_4, y_3)		0.99, -0.99	-1.29, -3.87	$\frac{-\sqrt{21}}{3}, -\sqrt{21}$	Saddle \rightarrow Sink
(x_4, y_4)		0.94, -2.37	-2.98, -0.75		Saddle \rightarrow Sink

Table 6: Values of λ and corresponding eigenvalues.

Flow Configurations:

- Default = 1
- Nordic Reversed = 2
- Labrador Reversed = 3
- Both reversed = 4

Equilibrium	λ			
	-1	-0.5	0.5	1
(x_1, y_1)		1	3	3
(x_1, y_2)		2	1	
(x_1, y_3)		1	1	1
(x_1, y_4)		1	1	
(x_2, y_1)		1	3	
(x_2, y_2)	3	3	1	
(x_2, y_3)		1	1	
(x_2, y_4)	1	1	1	
(x_3, y_1)		2	3	
(x_3, y_2)	4	4	1	
(x_3, y_3)		2	1	
(x_3, y_4)	2	2	1	
(x_4, y_1)		1	4	4
(x_4, y_2)		3	2	
(x_4, y_3)		1	2	2
(x_4, y_4)		1	2	

Table 7: Flow configurations for each equilibrium point at varying values of λ .

5.2.6 High Resolution Phase Portrait at Zero Salinity Flux

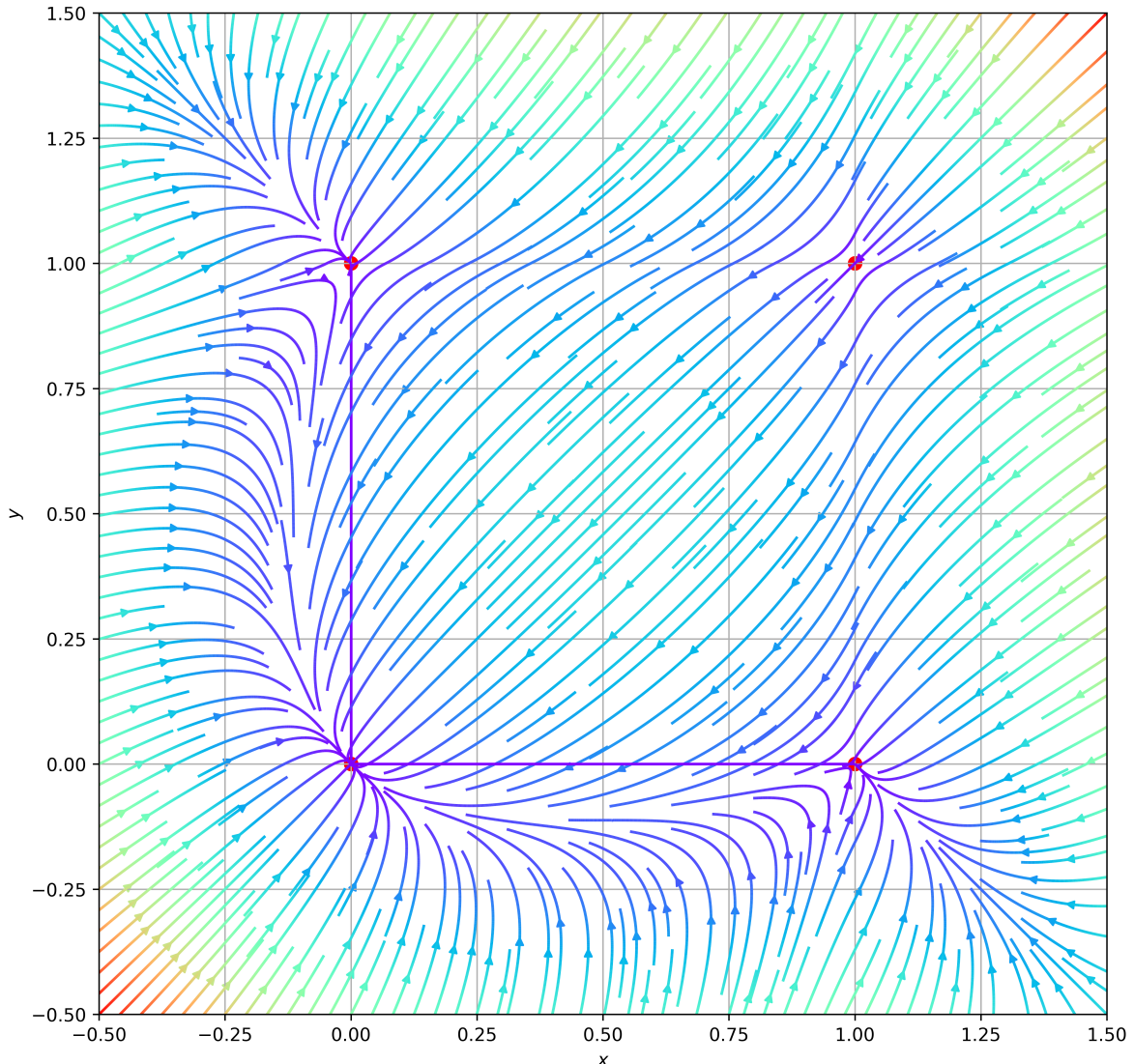


Figure 25: Phase portrait for nondimensionalised three box-model, with 0 salinity flux ($\psi = 0$). Equilibrium points marked in red at $(0,0)^T$, $(0,1)^T$, $(1,0)^T$, $(1,1)^T$

5.2.7 Bifurcation Figures

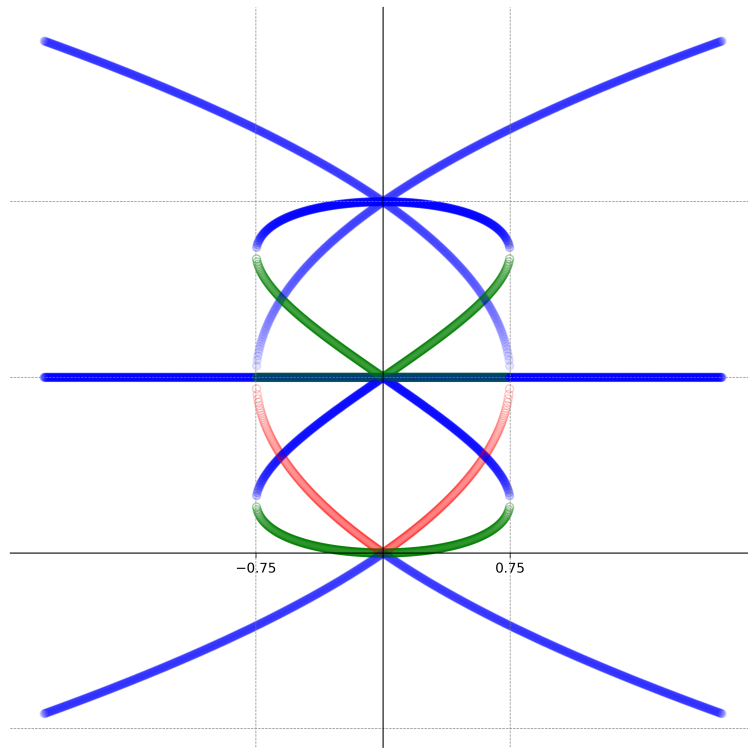


Figure 26: Detailed bifurcation diagram for our three box-model. Stable, unstable and saddle equilibria are shown in blue, red and green respectively. Note the equilibrium solution given by (x_3, y_1) as the green curve intersecting the origin.

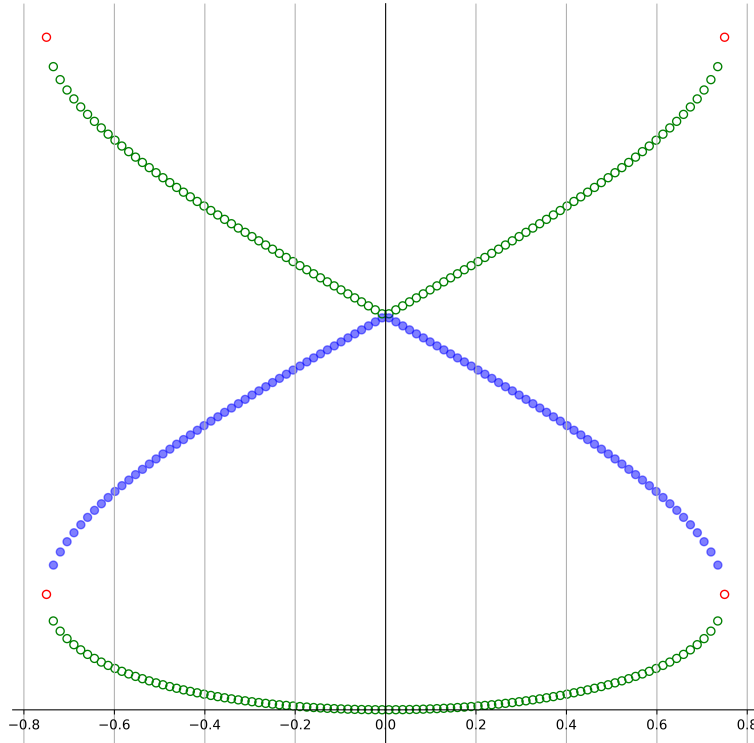


Figure 27: Reduced version of Figure 26. Only equilibrium solutions plotted are those of (x_1, y_2) , (x_2, y_1) and (x_3, y_1) with stable, unstable and saddle equilibria represented by blue filled, red unfilled and green unfilled points. Clear symmetry about the line $\lambda = 0$ by both (x_1, y_2) and (x_2, y_1) . Note the final equilibria points marked in red at $\lambda = \pm 3/4$. These equilibria each have eigenvalues $a, 0$ where $a < 0$. As such, their stability is ambiguous and this is still the case after calculating the *Jordan Form* of the Jacobian at these points 28.

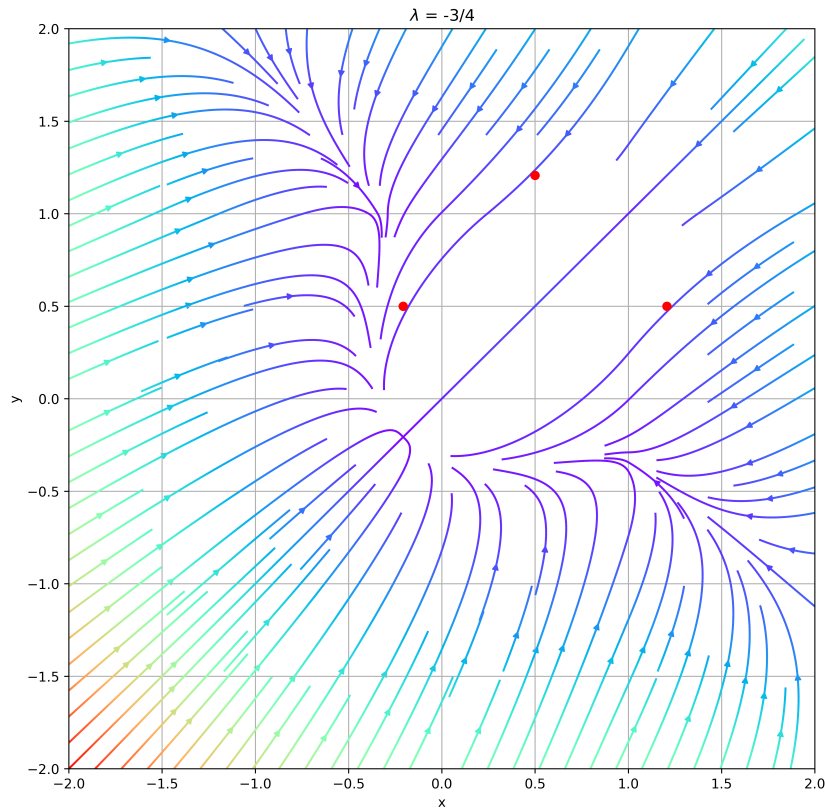


Figure 28: Phase portrait at $\lambda = -\frac{3}{4}$, with equilibrium points (x_3, y_1) , (x_1, y_2) and (x_2, y_1) marked in red.

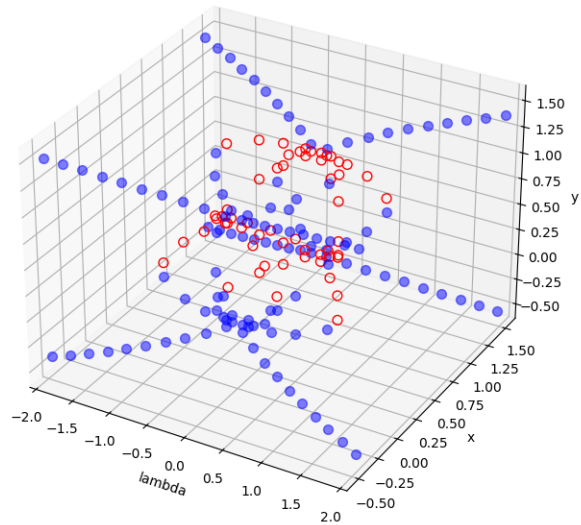


Figure 29: Three-dimensional bifurcation diagram. Stable equilibria shown as filled blue spheres, unstable equilibria shown as hollow red spheres.

Movement of Nullclines as a Function of λ

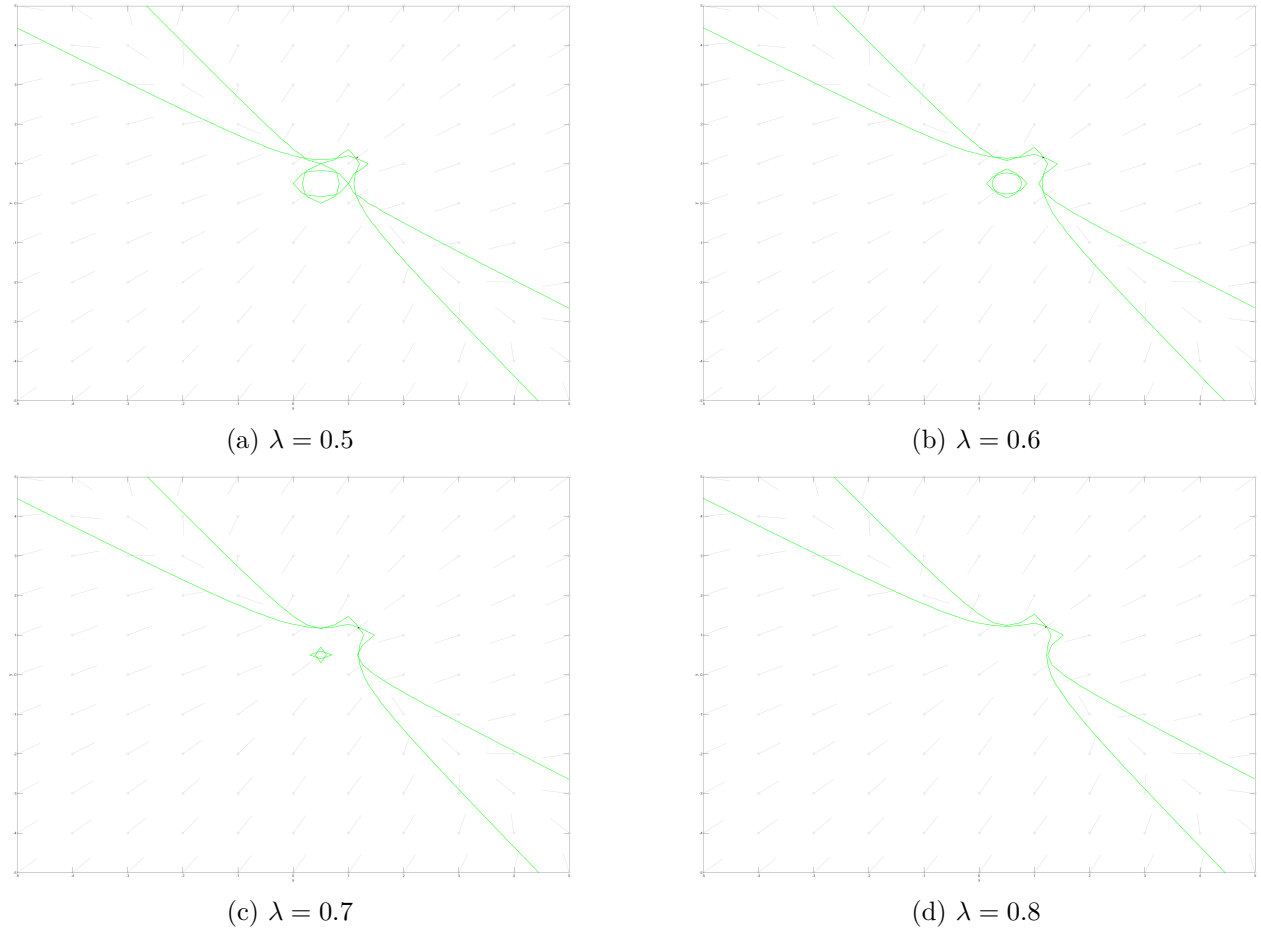


Figure 30: Nullcline progression as λ increases. Note the change between $\lambda = 0.7$ and $\lambda = 0.8$, where a set of nullclines ceases to exist, potentially representing saddle-node bifurcations as exhibited in both Stommel's [7] and Welander's [29].

5.3 GitHub Repository

The code for the calculations, finding equilibrium and making plots can be found in the following GitHub repository. <https://github.com/DavidMiles-Skov/gulf-stream-modelling/tree/main>